NOTICE: When government or other drawings, specifications or other data are used for any purpose other than in connection with a definitely related government procurement operation, the U. S. Government thereby incurs no responsibility, nor any obligation whatsoever; and the fact that the Government may have formulated, furnished, or in any way supplied the said drawings, specifications, or other data is not to be regarded by implication or otherwise as in any manner licensing the holder or any other person or corporation, or conveying any rights or permission to manufacture, use or sell any patented invention that may in any way be related thereto.

CATALOGED BY ASTIA
AS AD NO. 277640

SPOT COOLING AND HEATING OF SURFACES WITH HIGH VELOCITY IMPINGING AIR JETS

Part 1—Slot Jets on Plane Surfaces

BY

DARRYL E. METZGER

TECHNICAL REPORT NO. 52

PREPARED UNDER CONTRACT NONR 225(23)
(NR-090-342)
OFFICE OF NAVAL RESEARCH

DEPARTMENT OF MECHANICAL ENGINEERING
STANFORD UNIVERSITY
STANFORD, CALIFORNIA

277 640

ASTIA
RELEASED
JUL 12 1962
TISIA B

APRIL, 1962

SPOT COOLING AND HEATING OF SURFACES WITH HIGH VELOCITY IMPINGING AIR JETS

Part I - Slot Jets on Plane Surfaces

Technical Report No. 52

Prepared under Contract Nonr 225(23)
(NR-090-342)

For

Office of Naval Research

Reproduction in whole or part is permitted for
any purpose of the United States Government

Department of Mechanical Engineering
Stanford University
Stanford, California

April, 1962

Report Prepared By:

Darryl Eugene Metzger

Approved By:

A. L. London

Project Supervisor

ABSTRACT

Localized cooling of furnaces with jets of air is common in industry. The particular case of a small, high velocity slot jet impinging normally on a plane surface is studied experimentally by use of a transient method. The method is shown to be of use in determining local, as well as average, heat transfer coefficients. These results are presented in nondimensional form which will facilitate extension to fluids and slot dimensions other than those used in the tests.

Some limited results for circular jets are also included, and these are compared to the slot jet.

ACKNOWLEDGMENTS

The author wishes to thank Professor A. L London for his guidance. The financial support of the Office of Naval Research, Contract Nonr 225(23), is also appreciated.

TABLE OF CONTENTS

LIST OF FIGURES

LIST OF TABLES

REFERENCES

1. "Heat Transfer Between a Flat Plate and Jets of Air Impinging on It," by Robert Gardon and John Cobonpue, International Developments in Heat Transfer, 1961, Part II, pp 454 - 460.

2. "Heat Transfer Coefficients between Fluid Jets and Normal Surfaces," by J. M. F. Vickers, Industrial and Engineering Chemistry, Vol. 51, No. 8, August, 1959, pp. 967 - 972.

3. "Boundary Layer Theory," by Hermann Schlichting, Pergamon Press, 1955.

4. "Theoretical Hydrodynamics," by L. M. Milne-Thomson, The Macmillan Company, 1960.

5. Lecture Notes, W. M. Kays, Stanford University.

6. "Research During the Last Decade on Forced Convection Heat Transfer," by E. R. G. Eckert, International Heat Transfer Conference, 1961.

7. "The Plane Turbulent Wall Jet, Part 1. Jet Development and Friction Factor," by G. E. Meyers, J. J. Schauer, and R. H. Eustis, TR-No. 1, Contract NSF G9705, Department of Mechanical Engineering, Stanford University, 1961.

8. "The Plane Turbulent Wall Jet, Part 2. Heat Transfer," by G. E. Meyers, J. J. Schauer, and R. H. Eustis, TR-No. 2, Contract NSF G9705, Department of Mechanical Engineering, Stanford University, 1961.

9. "Fluid Meters, Their Theory and Application," American Society of Mechanical Engineers, 1959.

10. "On the Theory of Discharge Coefficients for Rounded-Entrance Flowmeters and Venturis," by M. A. Rivas, Jr., and A. H. Shapiro, Transactions of the ASME, Vol. 78, 1956, pp. 489 - 497.

11. "Hydrodynamic Entrance Lengths for Incompressible Laminar Flow in Rectangular Ducts," by L. S Han, Journal of Applied Mechanics, September, 1960, pp. 403 - 409.

12. "Compact Heat Exchanges," by W. M. Kays and A. L. London, National Press, 1955.

NOMENCLATURE

English Letter Symbols

A	throat area of nozzle, in^2
A_{leak}	surface area of target not exposed to the jet, in^2
A_{forced}	surface area of target exposed to the jet, in^2
b	slot jet width at nozzle exit, ft
$\overline{C}$	target thermal capacity, Btu/°F
c_p	specific heat, Btu/(lbm°F)
c	slot jet length at nozzle exit, ft
D	diameter of circular nozzle, ft
D_H	hydraulic diameter, ft
G	mass velocity at nozzle exit, $lbm/(hrft^2)$
g_c	proportionality factor in Newton's Second Law, 32.20 lbm-ft/(lbf-sec^2)
h	local heat transfer coefficient, $Btu/(hrft^{2\circ}F)$
h_{av}	average heat transfer coefficient, $Btu/(hrft^{2\circ}F)$
h_{leak}	average heat transfer coefficient on rear of target, $Btu/(hrft^{2\circ}F)$
K	the constant in Eq (12), dimensionless
k	thermal conductivity, Btu/(hrft°F)
ℓ	half length of rectangular target, radius of circular target, ft
L	throat length in nozzle, ft
P_a	ambient pressure, psia
P_n	plenum chamber pressure, psia

ΔP_n	pressure difference across nozzle, psi
P_∞	potential flow pressure along target surface, psia
q	heat flux, Btu/hr
R	thermal resistance, (hr°F)/Btu
t	model temperature, °F or millivolts
T	plenum chamber temperature, °R
u	velocity component in x-direction, ft/hr
U_o	average velocity at nozzle exit plane, ft/hr
U_∞	potential flow velocity along target surface in x-direction, ft/hr
U_ℓ	centerline velocity of jet at exit plane of nozzle, ft/hr
v	velocity component in y-direction, ft/hr
w_i	ideal flow rate through nozzle, lbm/hr
w_m	measured flow rate through nozzle, lbm/hr
x	coordinate along target surface, ft
y	coordinate normal to target surface, ft

Greek Letter Symbols

β	wedge angle, degrees
δ	nozzle to target distance, ft
ϕ	impingement angle, degrees
θ	time, sec
μ	viscosity, lbm/(ft hr)
ρ	density, lbm/ft^3

Non-Dimensional Quantities

C	nozzle discharge coefficient $\triangleq w_m/w_i$
m	Euler number $\triangleq (x\frac{\partial P_\infty}{\partial x})/(\rho U_\infty^2/2g_c)$
$N_{R,n}$	nozzle Reynolds number $\triangleq (GD_H)/\mu$
$N_{R,\ell}$	plate Reynolds number $\triangleq (G\ell)/\mu$
$N_{R,x}$	local plate Reynolds number for potential flow solution $\triangleq (U_\infty \rho x)/\mu$
N_{St}	local Stanton number $\triangleq h_{av}/(Gc_p)$
$N_{St,av}$	average Stanton number $\triangleq h_{av}/(Gc_p)$
$(N_{St,av})_{max}$	maximum $N_{St,av}$ as function of δ/b
N_{Nu}	local Nusselt number $\triangleq (hx)/k$
N_{Pr}	Prandtl number $\triangleq (\mu c_p)/k$
γ	aspect ratio of slot nozzle $\triangleq b/c$
Y_a	nozzle compressible flow coefficient in the flow metering equation

I INTRODUCTION

The use of impinging jets of air for cooling and heating purposes is common in industry. Thermal treatment of surfaces such as the toughening of glass are examples of such industrial applications. On a smaller scale, jets are used for spot cooling of electronic components and for thermal development of photographic films.

In general, two types of jets have been used: (1) the circular, or axial symmetric jets, and (2) the slot or two dimensional jet. One limiting case of the slot jet is that where the jet intersects the surface tangentially; this particular configuration has been called the "wall jet". Figures 1a, 1b, and 1c serve to describe these various jet types. The wall jet has been investigated both analytically and experimentally[7,8*] but no analytic treatment exists for the heat transfer characteristics of either the circular or slot jet at impingement angles greater than zero. The circular jet has been investigated experimentally by Gordon[1] and Vickers[2] for the case of normal impingement, $\phi = 90°$, and Gordon also studied arrays of circular jets impinging normally.

The present study arose out of a need for heat transfer coefficients for slot nozzles and is intended to help fill the gap in this area. The results herein are mainly concerned with slot nozzles in their most common applied configuration, 90° or normal impingement. This report also presents some limited results that were obtained with one size of circular jet impinging normally, but these are very limited and are given only to provide a preliminary comparison with the more complete slot jet results. Presented are the results of only the first part of a program which will eventually cover both

---

*Raised numerals denote References.

the slot and circular jets impinging at various angles on both plane and rounded surfaces.

It was decided to build an apparatus which would approximate "spot" or small area cooling and heating such as would be the case in the cooling of electronic components, for example. Thus, small, high velocity air jets were used, and the characteristic Reynolds numbers obtained based on the nozzle exit velocity and hydraulic diameter, were fairly small (less than 10,000 for the slot jets, and less than 20,000 for the one circular jet).

Figure 1d indicates the pertinent variables in the slot jet problem. The flow exits from a rectangular nozzle of width b and length c, travels as a free jet a distance δ before impinging normally onto a plane having a spot area $2b\ell$. Neglecting end effects, it can be anticipated that the heat transfer rate at a given distance from the stagnation point will be a function of the fluid dynamics involved and of the system geometry. Expressing this nondimensionally, for a constant Prandtl number fluid:

$$N_{St} = f(N_{R,n},\ x/b,\ \delta/b,\ \text{nozzle exit velocity profile}) \quad (1)$$

where

$$N_{St} \triangleq \frac{h}{Gc_p} \quad (2)$$

$$N_{R,n} \triangleq \frac{GD_H}{\mu} \quad (3)$$

$$N_{Pr} \triangleq \mu c_p/k = \text{constant}$$

The velocity profile at the nozzle exit plane must be included as a parameter since $N_{R,n}$ is based on the bulk average exit velocity and does not fully describe the jet.

For the average heat transfer over a distance ℓ from the stagnation point a similar correlation is expected:

$$N_{St,av} = f(N_{R,n}, \ell/b, \delta/b, \text{exit profile}) \tag{4}$$

where:

$$N_{St,av} \triangleq \frac{h_{av}}{Gc_p} \tag{5}$$

FIG. 1a

THE TWO-DIMENSIONAL OR SLOT JET

FIG. 1b

THE AXIAL SYMMETRIC OR CIRCULAR JET

FIG. 1c

THE WALL JET
A limiting case of the slot jet

FIG. 1d

NOMENCLATURE FOR SLOT JETS

FIG. 2a

BOUNDARY OF THE FINITE IMPINGING JET
Potential flow solution from Ref. 4

FIG. 2b

TWO DIMENSIONAL FLOW OVER A WEDGE

FIG. 2c

NORMAL IMPINGEMENT, $\beta = \pi$, $m = 1$

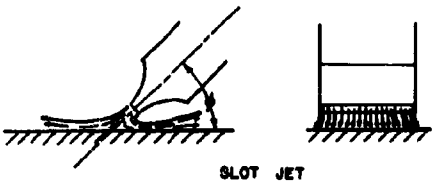

FIG. 1a

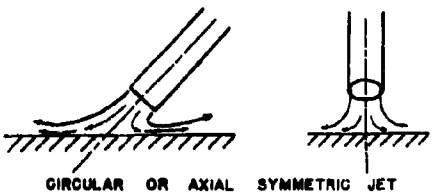

FIG. 1b

FIG. 1c

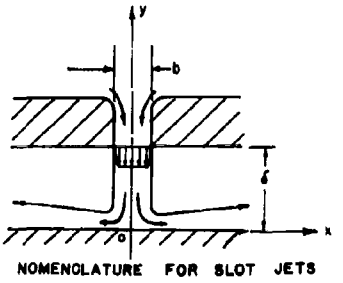

FIG. 1d

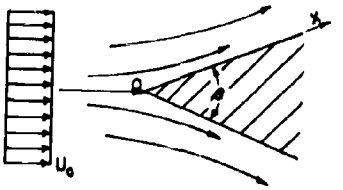

FIG. 2a

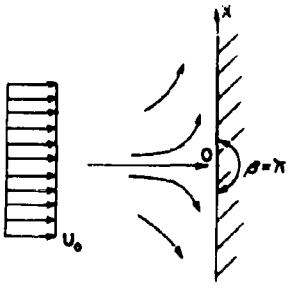

FIG. 2b

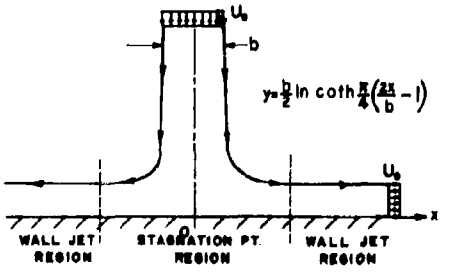

FIG. 2c

II ANALYSIS

The available analytical treatments relating to impinging jets are restricted to fluid dynamics considerations and only for the stagnation point region. A classical solution for the case of a viscous jet of infinite extent striking a plate at right angles was given by Schlichting[3]. He found the same velocity gradient in both the x and y direction; that is, $u = ax$ and $v = ay$. The nature of the solution is such that the velocity gradient, a, is indeterminate.

Milne-Thomson[4] has found a solution for the case of a finite inviscid slot jet striking a plate. He was able to obtain the equation for the boundary of the jet as it strikes and is turned by the plate. His equation for the boundary is as follows:

$$y = \frac{b}{2} + \frac{b}{\pi} \ell n \coth \frac{\pi}{4} \left(\frac{2x}{b} - 1\right) \qquad (6)$$

This is pictured in Fig. 2a.

With the free jet boundary specified, La Place's equation describing the flow could be solved by numerical means to check the correspondence between the velocity gradients in Schlichting's solution and those for the finite inviscid jet.

The velocity gradient in the potential core of the impinging jet is important since Eckert[5,6] has obtained a family of laminar flow solutions for heat transfer in the case of constant Euler number flow. Constant Euler number occurs for flow over a two dimensional wedge as shown in Fig. 2b. The potential flow velocity along the surface of the wedge varies as x^m where m is the Euler number and is a function of the wedge angle, β. The heat transfer for constant wall temperature is given by:

$$N_{Nu} = 0.56 \frac{\left[\frac{2m}{1+m} + 0.2\right]^{0.11}}{2 - \frac{2m}{1+m}} N_{Pr}^{\left(0.35 + \frac{0.04m}{1+m}\right)} N_{R,x}^{0.5} \quad (7)$$

where $$N_{Nu} \triangleq \frac{hx}{k} = N_{St} \cdot N_{Pr} \cdot N_{R,x} \quad (8)$$

$$N_{R,x} \triangleq \frac{U_\infty \rho x}{\mu} \quad (9)$$

For $\beta = \pi$, $m = 1$, and the inviscid flow reduces to that given by Schlichting; that is, $u = ax$. Equation (7) then reduces to:

$$N_{Nu} = 0.57 N_{Pr}^{0.37} N_{R,x}^{0.50} \quad (10)$$

In lieu of solving La Place's equation for the finite jet as defined by Milne-Thomson, we will assume that a constant velocity gradient in the x-direction does exist in the finite jet. This is probably a good assumption near the stagnation point.

Then: $$U_\infty = ax \quad (11)$$

An approximate value of the velocity gradient, a , may be extracted from Milne-Thomson's solution by noting that the flow area after the turning of the jet is complete is the same as the original flow area. Thus, from consideration of the continuity of the flow, the mean velocity after complete turning is equal to the mean velocity, U , which prevailed before turning.

Thus we can express (11) as:

$$U_\infty = \frac{U}{Kb}\, x \qquad (12)$$

where K is a constant.
Using the approximation (12), one can rearrange (10) from

$$\frac{hx}{k} = 0.57\, N_{Pr}^{0.37} \left(\frac{x\, U_\infty \rho}{\mu}\right)^{0.5}$$

to $$\frac{hD_H}{k} = 0.57\, N_{Pr}^{0.37}\, D_H \left(\frac{U\,\rho}{Kb\mu}\right)^{0.5}$$

For the slot nozzle:

$$D_H = \frac{2bc}{b+c}$$

and for narrow slots $b \ll c$ so

$$D_H \simeq 2b$$

Thus

$$\frac{hD_H}{k} = 0.57 \left(\frac{2}{K}\right)^{0.5} N_{Pr}^{0.37} \left(\frac{U\rho D_H}{\mu}\right)^{0.5}$$

But

$$\frac{hD_H}{k} = \left(\frac{h}{Gc_p}\right)\left(\frac{GD_H}{\mu}\right)\left(\frac{\mu c_p}{k}\right) = N_{St}\, N_{R,n}\, N_{Pr}$$

Then

$$N_{St}\, N_{R,n}^{1/2} = \text{constant} \cdot N_{Pr}^{-0.63} \qquad (13)$$

and for any given Prandtl number, we would expect the heat transfer in the vicinity of the stagnation point (where (11) may be a valid assumption) to correlate as

$$N_{St}\, N_{R,n}^{1/2} = \text{constant} \qquad (14)$$

Note the correspondence between (14) and the expected correlation as given in (1). The above analysis neglects any effects of δ/b and the nozzle exit velocity profile. The parameter x/b is included in the analysis in that (14) is expected to correlate the data at values of x/b near the stagnation point.

Equation (14) provides a basis for the correlation of the experimental results in Section VI.

III EXPERIMENTAL METHOD: THE TRANSIENT TECHNIQUE

The transient method for determining the convective conductance of the jet consists simply of recording the transient temperature response of an initially heated model as a result of jet cooling. A simple analysis is then used to relate this transient to the conductance through a thermal circuit as shown in Fig. 3b. It should be noted that Fig. 3b pictures the distributed thermal resistance and capacitance as being "lumped" into a single RC circuit. The criteria for this lumping is as follows:

$$R_{\text{convective film}} \gg R_{\text{model}}$$

and (15)

$$\overline{C}_{\text{model}} \gg \overline{C}_{\text{convective film}}$$

The models used in the experimental work were designed so that these criteria were satisfied. Figure 3a shows a typical flat plate model. A small (1/2" x 1/2" x 1/4") copper block is mounted flush into a balsa wood block which both supports the model and extends the plane target surface. There is a small back-side heat leak in addition to the predominate jet convection on the front surface as shown in Fig. 3c. The calibration of this back-side leakage is discussed in Appendix B.

The relation between the transient response and the average jet conductance, h_{av}, is developed below. Referring to Fig. 3c, the heat flux, q, is related to the temperature difference through a rate equation:

$$q_{\text{total}} = (1/R_{\text{total}})(t_{\text{plate}} - t_{\text{air}})$$

If we specify $t_{\text{air}} = 0$ as a datum temperature:

$$q_{\text{total}} = (1/R_{\text{total}})\, t_{\text{plate}}$$

This flux is related to the loss in thermal energy in the model by an energy balance:

$$q_{total} = - \overline{C} \frac{dt_{plate}}{d\theta}$$

Combining the two equations and integrating the result.

$$1/R_{total} \int_{\theta_o}^{\theta} d\theta = - \overline{C} \int_{t_o}^{t} \frac{dt_{plate}}{t_{plate}}$$

$$1/R_{total} \, (\theta - \theta_o) = - \overline{C} \, \ell n \, t_{plate} \Big]_{t_o}^{t}$$

Let $\theta_o = 0$ when $t_{plate} = t_o$ and note that:

$$1/R_{total} = 1/R_{forced} + 1/R_{leak} = (hA)_{forced} + (hA)_{leak}$$

Thus

$$(hA)_{forced} = - \frac{\overline{C}}{\theta} \ell n(t/t_o) - (hA)_{leak}$$

or

$$h_{forced} \, (= h_{av}) = - \left(\frac{\overline{C}}{\theta A_{forced}}\right) \ell n \left(\frac{t}{t_o}\right) - h_{leak} \left(\frac{A_{leak}}{A_{forced}}\right) \tag{16}$$

The conductance, h_{forced}, evaluated by (16), is the average heat transfer coefficient, h_{av}, averaged with respect to surface area over the whole length, 2ℓ, of the model. One shortcoming of the transient method heretofore has been that it was useful only for evaluating average heat transfer coefficients. The next section describes how the method may be extended quite simply to yield local heat transfer coefficients.

FIG. 3a

SCHEMATIC OF TYPICAL TARGET ASSEMBLY

FIG. 3b

BASIC THERMAL CIRCUIT

FIG. 3c

THERMAL CIRCUIT WITH BACK SIDE HEAT LEAK

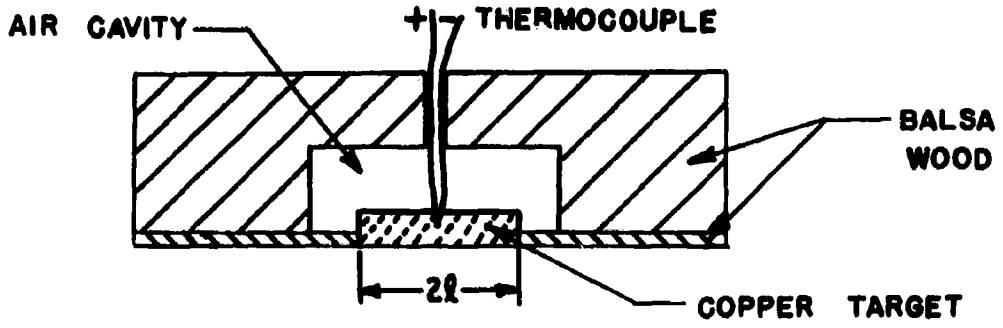

FIG. 3a

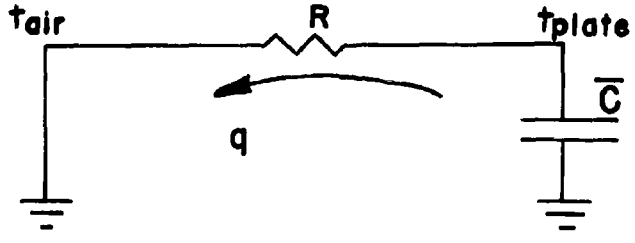

FIG. 3b

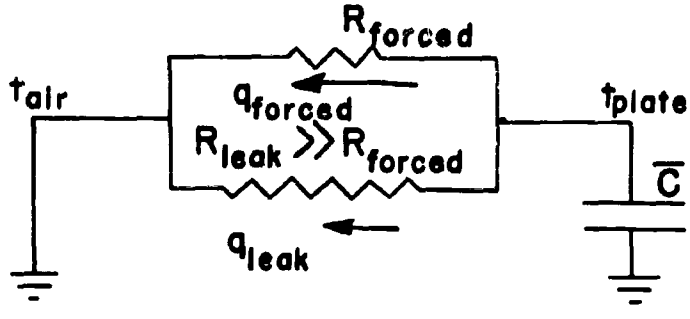

FIG. 3c

IV EXTENSION OF THE TRANSIENT TECHNIQUE FOR OBTAINING LOCAL HEAT TRANSFER COEFFICIENTS

The foregoing method of analysis of the transient response may be extended to yield local coefficients by noting that the average Stanton number over the flow length $0 - x$ on the plate is given by:

$$N_{St_{av,x}} \triangleq \frac{1}{x} \int_0^x N_{St}\, dx \tag{17}$$

Therefore:

$$\frac{d}{dx}\left(N_{St_{av,x}} \cdot x\right) = N_{St}$$

and

$$N_{St} = N_{St_{av,x}} + x \left(\frac{dN_{St_{av,x}}}{dx}\right)_x$$

Thus

$$\left(N_{St}\right)_{x=\ell} = N_{St_{av,\ell}} + \ell \left(\frac{dN_{St_{av,x}}}{dx}\right)_{x=\ell} \tag{18}$$

In terms of the anticipated correlation of the results as given by (1), the question is how does the local N_{St} vary with increasing x/b, with all the other parameters held constant. To illustrate the application of Eq. (18), consider the following example. Four targets of different lengths, ℓ, are available and identical flow rates from the same nozzle at the same distance, δ, are directed at each of them in turn. Then $N_{R,n}$, δ/b, and the nozzle exit profile will have constant values for the four tests. The results of these tests can be plotted as in Fig. 4a. A faired curve through the test points provides the variation

in $N_{St_{av,\ell}}$ with increasing ℓ/b, at a constant value of $N_{R,n}$ and δ/b. The local heat transfer, N_{St}, at any distance ℓ from the stagnation point may be obtained from this curve by graphically evaluating the ordinate and the derivative

$$(N_{St,av})_{x=\ell} \quad \text{and} \quad \left(\frac{dN_{St,av}}{dx}\right)_{x=\ell}$$

Figure 4b illustrates how the results of Fig. 4a may be obtained in an equivalent manner with only one target of length ℓ, instead of four as just considered, by varying the nozzle width, b. Of course variation of b means a variation of nozzle exit area and thus the flow rate through the nozzle has to be changed so as to maintain a constant $N_{R,n}$. This extension to the method of Fig. 4b, that is, obtaining local coefficients indirectly on a nondimensional basis, requires that one have confidence in the proposed correlation of $N_{St,av}$ as predicted in (1) and that the experimental scatter be small. In section VI confidence in the correlation is built up through the results of successive experiments, and then these results are used to extract the local heat transfer values.

FIG. 4a

$N_{St,av}$ VERSUS ℓ/b OBTAINED BY VARYING TARGET SIZE

FIG. 4b

$N_{St,av}$ VERSUS ℓ/b OBTAINED BY VARYING NOZZLE SIZE

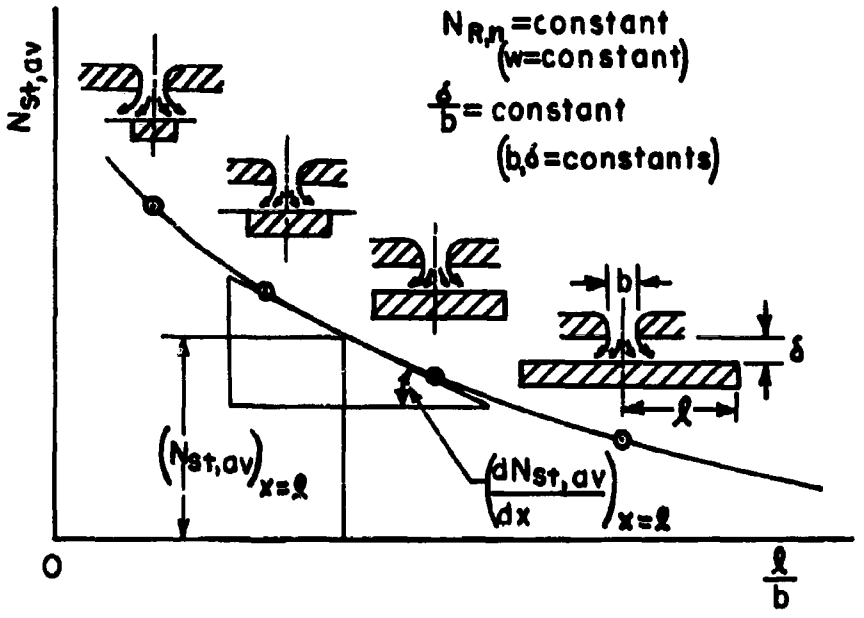
$N_{R,n}$=constant
(w=constant)
$\frac{\delta}{b}$= constant
(b,δ=constants)
$N_{St,av}$
b
δ
ℓ
$(N_{st,av})_{x=\ell}$
$\left(\frac{dN_{St,av}}{dx}\right)_{x=\ell}$
0
$\frac{\ell}{b}$

FIG. 4 a

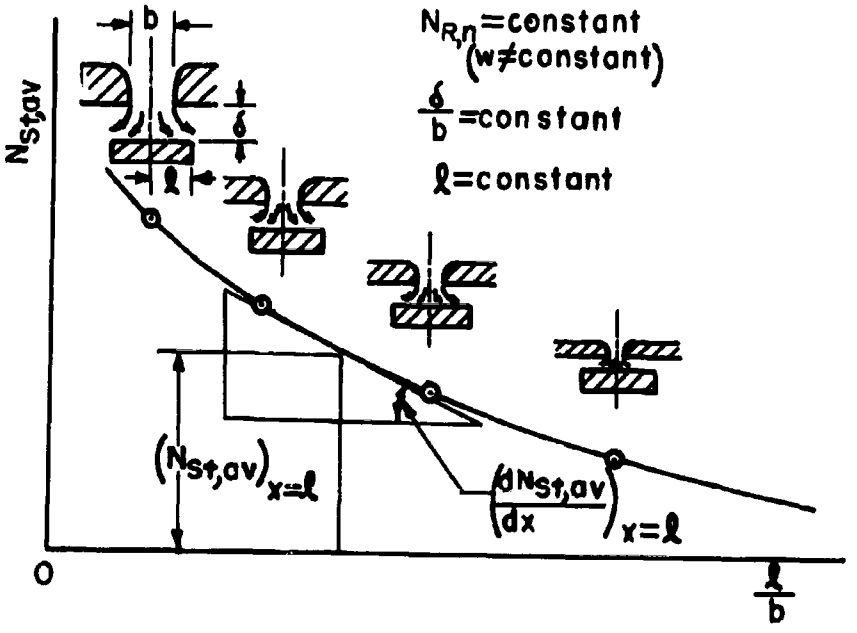
$N_{R,n}$=constant
(w≠constant)
$\frac{\delta}{b}$=constant
ℓ=constant
$N_{St,av}$
b
δ
ℓ
$(N_{St,av})_{x=\ell}$
$\left(\frac{dN_{St,av}}{dx}\right)_{x=\ell}$
0
$\frac{\ell}{b}$

FIG. 4 b

V EXPERIMENTAL APPARATUS

A schematic of the overall experimental apparatus is shown in Fig. 5. Air is supplied from a compressor through a combination of receivers and pressure regulators to the flow metering section which consists of a rotameter for measuring the flow rate and a 100-inch mercury manometer for measuring the rotameter inlet pressure. The air is then directed into the nozzle plenum chamber through a needle valve which is used to set the flow rate. The plenum chamber contains screens for straightening and quieting the flow and is topped by the nozzle block assembly for slot nozzles and the nozzle plate for round nozzles. An air tight joint is assured between the plenum and nozzle block plate by use of an O-ring seal.

The nozzle block and nozzles are shown in the photographs of Fig. 6. Three sets of nozzles were used to evaluate the effect of the nozzle exit velocity profile on the heat transfer characteristics of the jet. The design of these nozzles is covered in Appendix A. They are all 0.75 inch wide and slide in a groove machined in the nozzle block. All three sets of nozzles are interchangeable in the same nozzle block. The nozzle (and thus the jet) thickness is adjustable and the dimensions b used in the tests were 0.010, 0.020, 0.040, 0.060 and 0.080 inch. These were set with the use of precision thickness gages.

The close clearance machining of the nozzles and block allowed very adequate sealing with a thin film of grease between the sliding surfaces and insured that all the metered flow actually passed through the nozzle. An additional check on the equality of flow passing through the rotameter and nozzle is furnished by the calibration of the nozzles as a flow metering device. This calibration is covered in Appendix A. For every test run taken the flow

rate measured by the rotameter was checked against that computed to be passing through the nozzle. The rotameter has been calibrated against a standard orifice and is known to be accurate to $\pm$ 1% in the range used.

Two targets were used in the slot nozzle tests: one of ℓ = 0.50 inch, the other of ℓ = 0.25 inch. These are mounted in balsa wood supports so that they present an aerodynamically clean surface for the impinging jet. A thermocouple is mounted in the center of each target and is placed in series with a thermocouple in the plenum chamber below the jet. The voltage across the leads is thus proportional to the difference in temperature between the target and the air in the plenum. This voltage is measured with a self balancing potentiometer.

The relative alignment and positioning of the nozzle and target is achieved accurately through the use of two rotary micrometer tables; one to hold the target, and one to hold the nozzle assembly. These tables are commonly called rotary cross-feed tables and are used for positioning and feeding in machining operations. With the use of these tables, relative positions can be set accurately to a thousandth of an inch, and provision is built in for tilting the target to impingement angles less than 90°. Figure 7 shows the complete positioning assembly. The photograph of Fig. 8 shows the entire experimental setup.

FIG. 5

SCHEMATIC OF EXPERIMENTAL APPARATUS

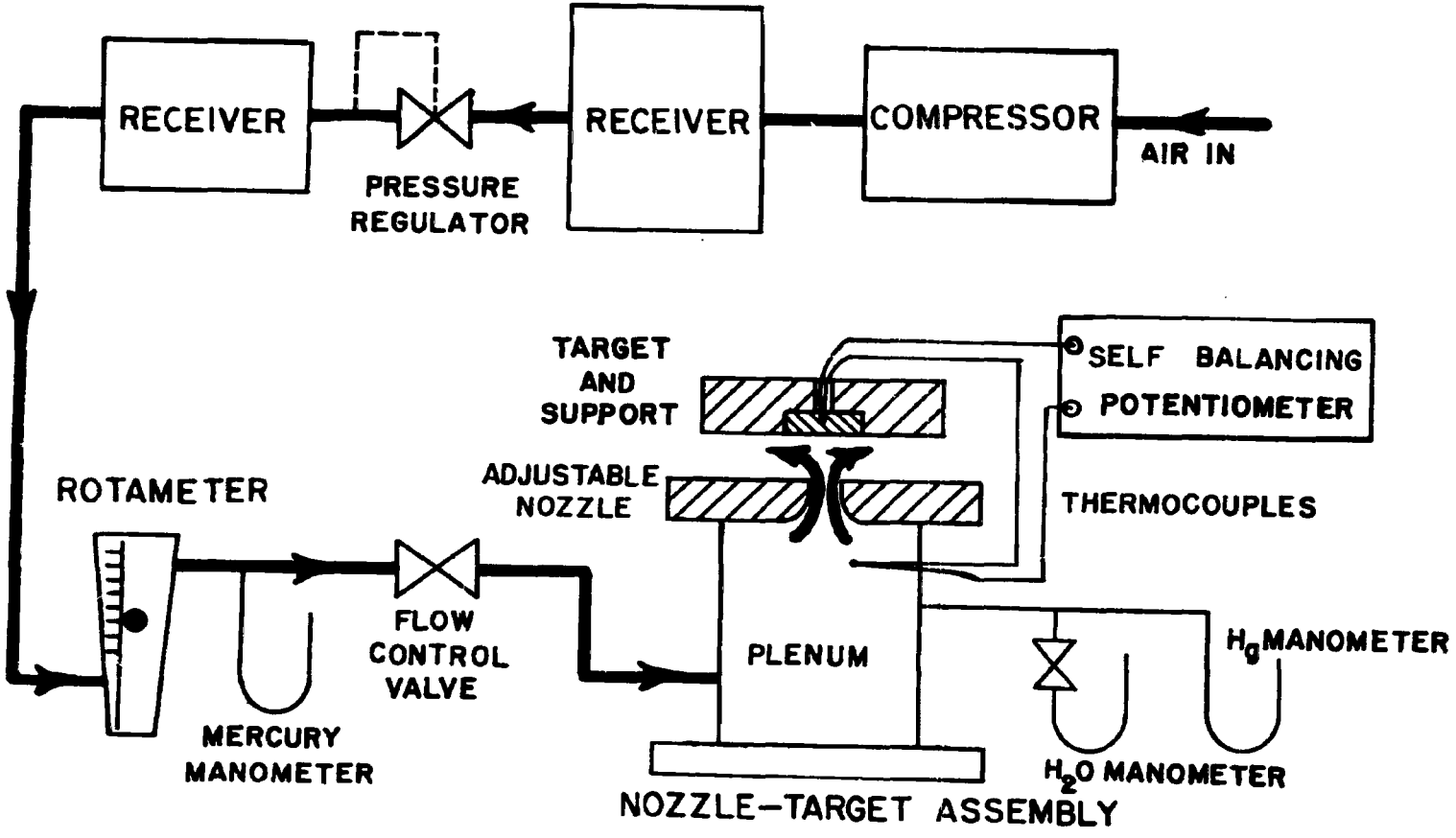
RECEIVER
PRESSURE REGULATOR
RECEIVER
COMPRESSOR
AIR IN
TARGET AND SUPPORT
SELF BALANCING POTENTIOMETER
ADJUSTABLE NOZZLE
THERMOCOUPLES
ROTAMETER
FLOW CONTROL VALVE
PLENUM
H_g MANOMETER
MERCURY MANOMETER
H_2O MANOMETER
NOZZLE–TARGET ASSEMBLY

FIG. 5

FIG. 6

PHOTOGRAPHS OF NOZZLES AND

NOZZLE ASSEMBLY

(See Fig. 21 for dimensions)

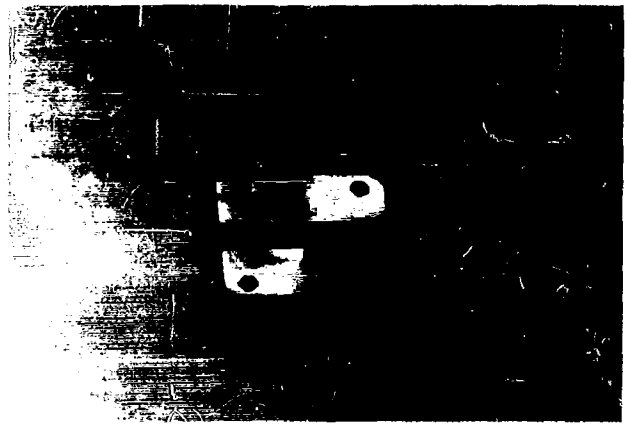

NOZZLE BLOCK AND NOZZLES TOP VIEW

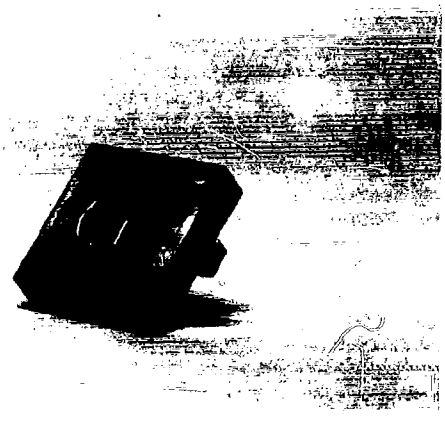

NOZZLE BLOCK AND NOZZLES BOTTOM VIEW

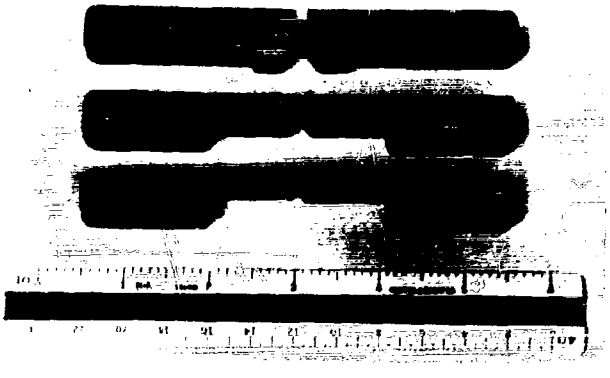

SLOT NOZZLES

FIG. 6

FIG. 7

PHOTOGRAPH OF ROTARY TABLES,

NOZZLE AND TARGET

The inset shows the 1 inch (ℓ = 0.50 inches)

rectangular target assembly

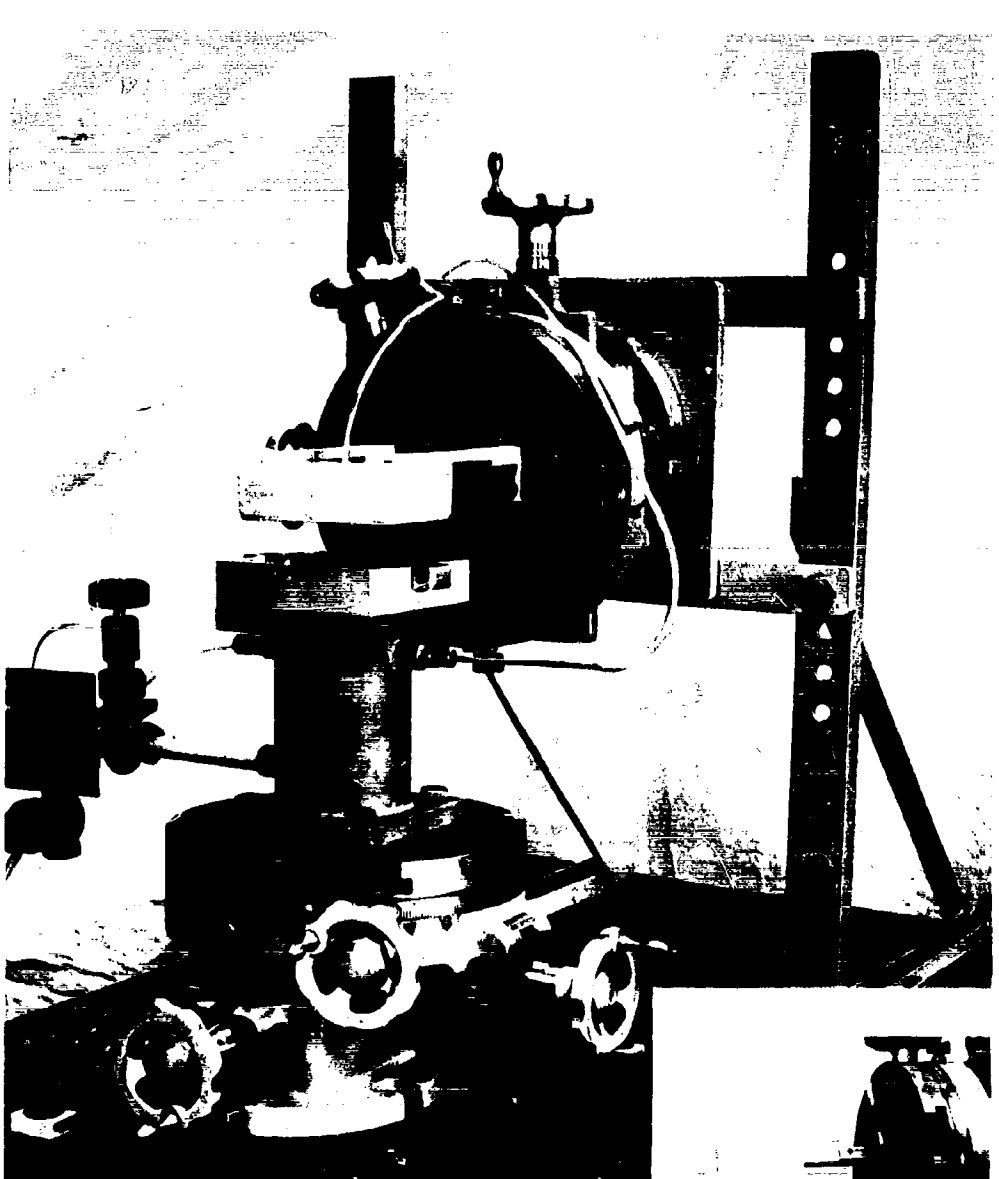

FIG. 7

FIG. 8

PHOTOGRAPH OF COMPLETE EXPERIMENTAL SET UP

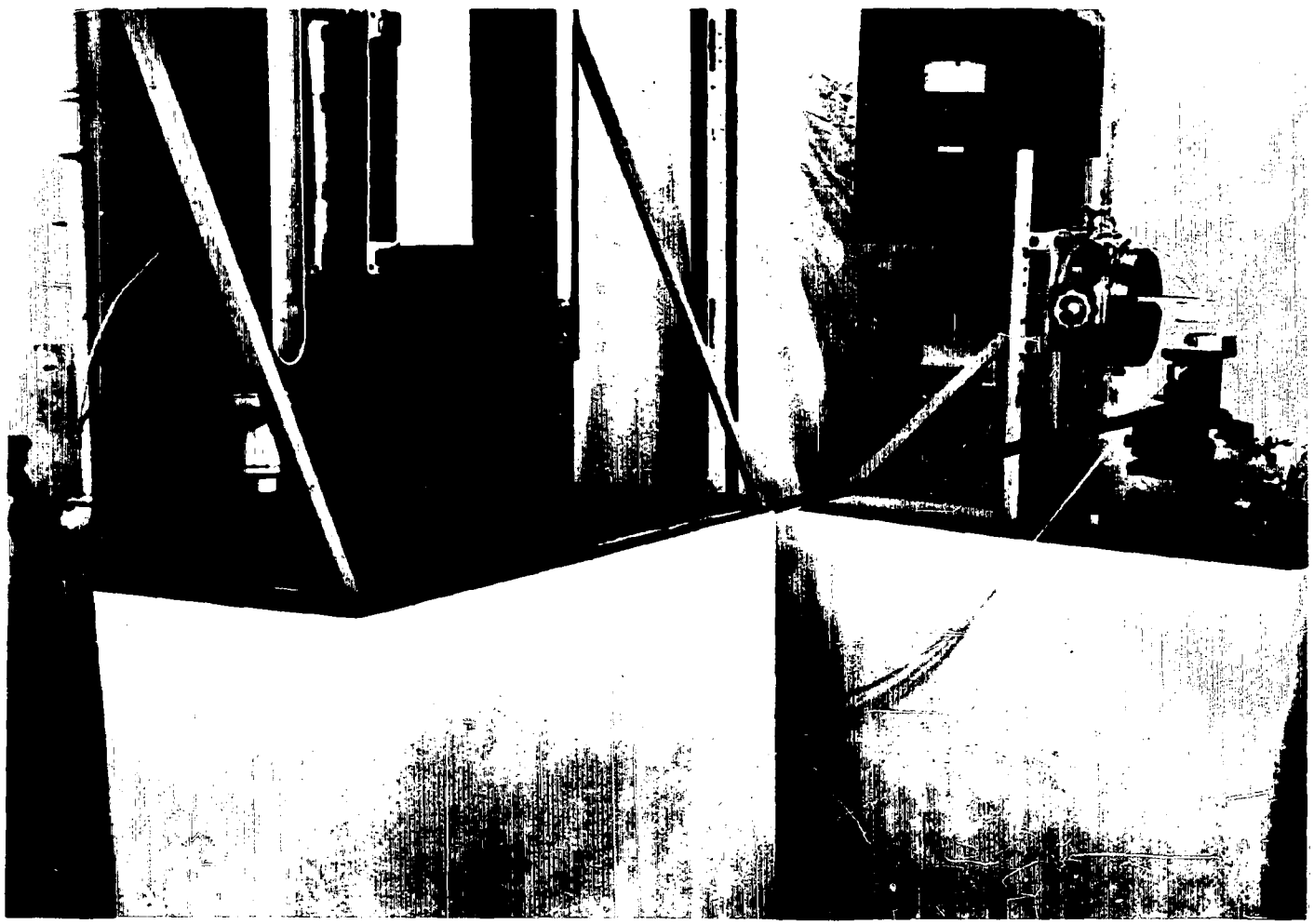

FIG. 8

VI EXPERIMENTAL RESULTS

A series of tests were conducted to systematically investigate the influence of the independent nondimensional parameters entering into the proposed correlation equation (1).

Effect of Nozzle-to-Target Distance, δ/b

The first series of tests were designed to obtain the effect of the geometrical parameter, δ/b, on $N_{St,av}$, all other parameters held constant. A rather peculiar effect is apparent from these tests. The average heat transfer rate over the target is at a maximum at δ/b around 8 and decreases with δ/b smaller than 8 and larger than 8. The results of a large number of tests are given in Fig. 9 in the form of $N_{St,av}/(N_{St,av})_{max}$ vs. δ/b where $(N_{St,av})_{max}$ is the maximum value of $N_{St,av}$ attained as a function of δ/b. The surprising aspect is, of course, the drop off in heat transfer for small δ/b ratios. This effect is apparent throughout the entire range of $N_{R,n}$ (3,000 to 10,000) and ℓ/b (3.125 to 50). This peaking is greater for small ℓ/b ratios, which indicates that it is a phenomenon associated with the heat transfer near the stagnation point. The average heat transfer obtained with small ℓ/b ratios is, of course, dominated by the heat transfer near the stagnation point, while that obtained for large ℓ/b ratios is dominated by the wall jet region. The stagnation point region and wall jet region are described in Fig. 2c.

This reduction in heat transfer coefficient for small nozzle-to-target distances is similar to that observed by Gordon[1] for circular jets. The free jet, after leaving the nozzle, is constantly entraining the surrounding fluid; as far as the jet heat transfer is concerned, it appears that this entrainment is initially beneficial and then detrimental

with further increase in δ/b beyond 10.

For the range of parameters attainable with the present apparatus, a nozzle placed at $\delta/b = 8$ appears to yield heat transfer coefficients no lower than 95% of the maximum attainable at other values of δ/b. Since, for design purposes, one is interested in maximum heat transfer rates, it was decided to make all further tests at a constant value of $\delta/b = 8.0$ and correlate the results on this basis. In the range $7<\delta/b<10$ no significant variation of the heat transfer coefficient will result as is evident from Fig. 9.

Effect of Target Size, ℓ/b

At the fixed nozzle-to-plate distance ratio, $\delta/b = 8.0$, tests were taken with the two targets ($\ell = 0.5$ and 0.25 inch), and the ℓ/b ratio was varied for each model by varying the nozzle thickness, b. For these tests the flow rate was adjusted so as to maintain a constant value of $N_{R,n}$. Figure 10 shows the results of these runs graphically. It should be noted that with this scheme of testing it is possible, by the use of two targets of different size, to obtain test results with identical values of $N_{R,n}$, ℓ/b, and δ/b and yet obtain these results with different values of ℓ, b, and flow rate. As seen in Fig. 10, these results correlate very well, within the experimental uncertainty, which lends confidence to the anticipated correlation of (1).

It should be noted at this time that the nozzle exit velocity profile included in (1) has not been mentioned so far because this parameter was found to have a very minor effect on the heat transfer results. Further discussion of this point will be presented later.

The lower curve of Fig. 10, that is, $N_{R,n} = 7400$ was also repeated at several values of δ/b to further illustrate the effect of this parameter. These results are shown in Fig. 11.

FIG. 9

EFFECT OF NOZZLE-TO-TARGET DISTANCE, δ/b, ON $N_{St,av}$

(See Table 7 for tabulated results)

$\phi = 90°$

FIG. 10

EFFECT OF TARGET SIZE, ℓ/b ON $N_{St,av}$ AT CONSTANT $N_{R,n}$

(See Table 8 for tabulated results)

$\delta/b = 8.0$

$\phi = 90°$

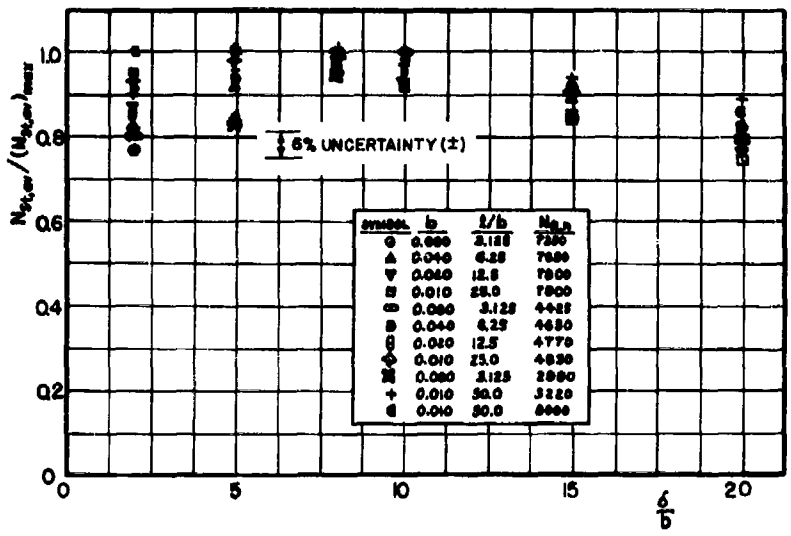
6% UNCERTAINTY (±)
1.0
0.8
0.6
0.4
0.2
0
0
5
10
15
20
δ/b

FIG. 9

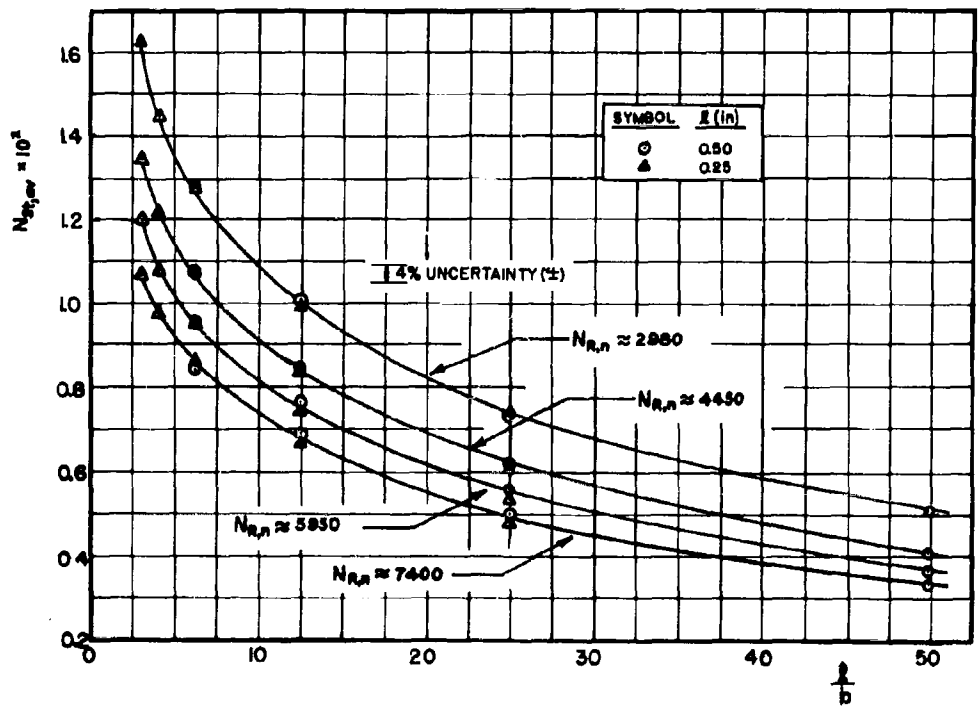
SYMBOL
δ (in)
0.50
0.25
4% UNCERTAINTY (±)
N_R,n ≈ 2980
N_R,n ≈ 4450
N_R,n ≈ 5850
N_R,n ≈ 7400
1.6
1.4
1.2
1.0
0.8
0.6
0.4
0.2
0
10
20
30
40
50
b

FIG. 10

Additional insight into the effect of ℓ/b may be had by correlating the data in a somewhat different manner using $N_{R,\ell}$ instead of $N_{R,n}$. In Fig. 10, the data is correlated on the basis of (1): that is,

$$N_{St,av} = f(N_{R,n}, \ell/b, \delta/b) \tag{19}$$

However, $N_{R,n}$ and ℓ/b may be combined into a Reynolds number based on the flow length along the plate as follows:

$$N_{R,n}\left(\frac{\ell}{b}\right) = \frac{GD_H}{\mu}\left(\frac{\ell}{b}\right) = \frac{\left(\frac{w}{bc}\right)\left(\frac{2bc}{b+c}\right)\left(\frac{\ell}{b}\right)}{\mu}$$

For the narrow slot nozzles used, $b<<c$; therefore, $(b+c) \simeq c$. Thus

$$N_{R,n}\left(\frac{\ell}{b}\right) \simeq \frac{2w}{\mu c}\left(\frac{\ell}{b}\right) = 2\,\frac{G\cdot\ell}{\mu} \triangleq 2N_{R,\ell}$$

$$\text{or} \qquad N_{R,\ell} \simeq \frac{N_{R,n}}{2}\left(\frac{\ell}{b}\right) \tag{20}$$

A functional relationship equivalent to (19) is thus:

$$N_{St,av} = f(N_{R,\ell}, \ell/b, \delta/b) \tag{21}$$

The same results as previously presented in Fig. 10 are graphed in Fig. 12 according to (21) as $N_{St,av}$ versus $N_{R,\ell}$. The reference line shown in Fig. 12 is the Pohlhausen solution for heat transfer from a flat plate at zero incidence ($\phi = 0$) to an infinite stream with a laminar boundary layer. It can be seen that on this basis the parameter ℓ/b has a rather minor effect in the range tested ($3.125<\ell/b<50$). Also, it is significant that these results for normal

FIG. 11

EFFECT OF NOZZLE TO TARGET DISTANCE δ/b,

ON $N_{St,av}$ VERSUS ℓ/b CURVES

(See Table 9 for tabulation results)

$N_{R,n} \approx 7400$

$\phi = 90°$

FIG. 12

$N_{St,av}$ VERSUS $N_{R,\ell}$

$\phi = 90°$

$\delta/b = 8.0$

The Pohlhausen solution for a laminar boundary layer on a flat plate at $\phi = 0°$ is shown as a dotted line.

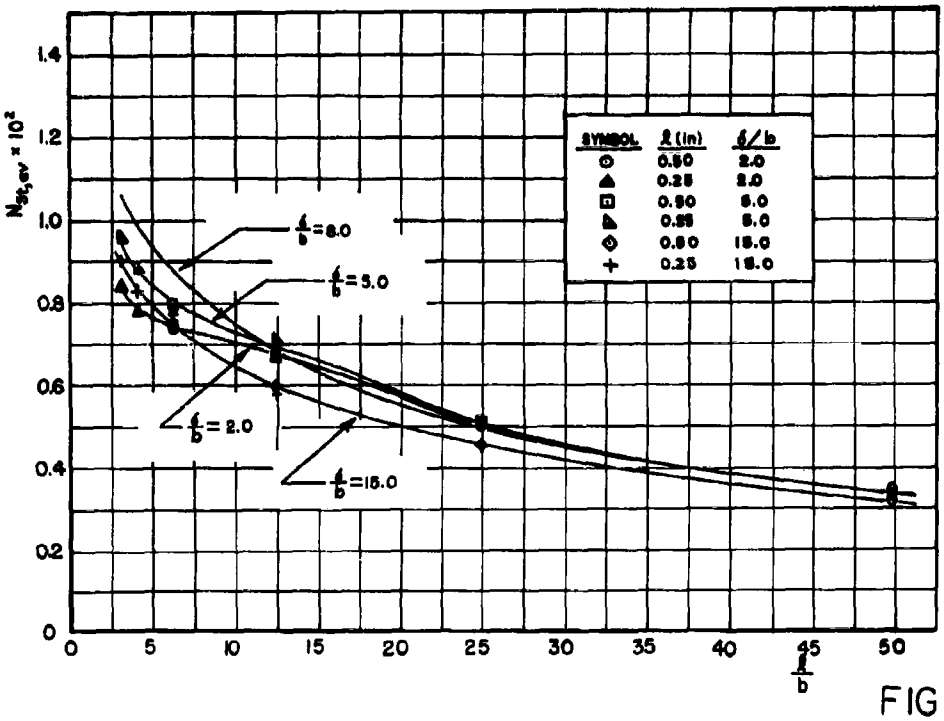
SYMBOL
ℓ (in)
ℓ/b
0.50
2.0
0.25
2.0
0.50
5.0
0.25
5.0
0.50
15.0
0.25
15.0
ℓ/b=8.0
ℓ/b=5.0
ℓ/b=2.0
ℓ/b=15.0
N_St,ev x 10²
ℓ/b

FIG. 11

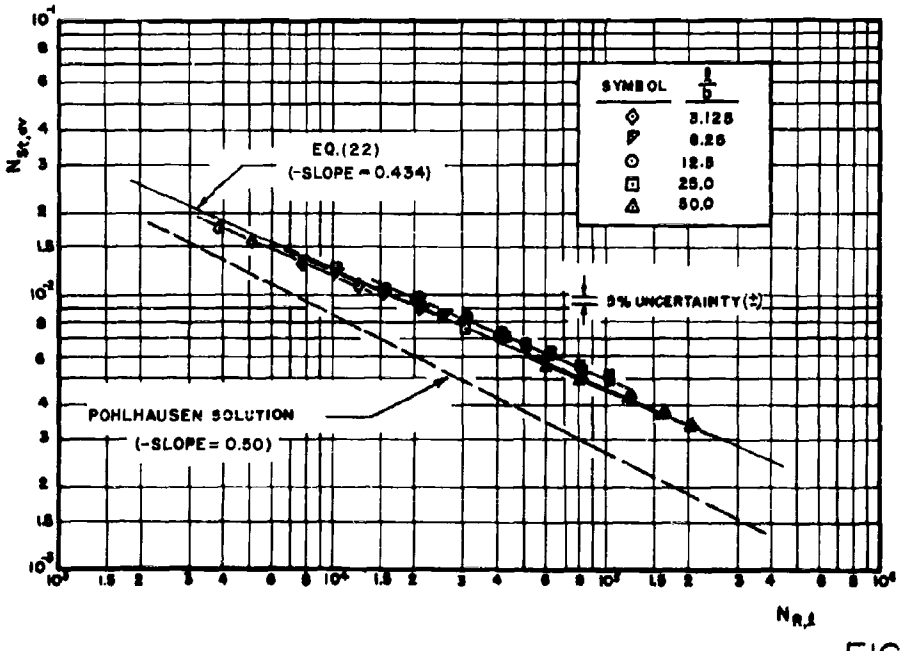
SYMBOL
ℓ/b
3.125
6.25
12.5
25.0
50.0
EQ.(22)
(-SLOPE = 0.434)
5% UNCERTAINTY (±)
POHLHAUSEN SOLUTION
(-SLOPE = 0.50)
N_St,ev
N_R,ℓ

FIG. 12

impingement ($\phi = 90°$) indicate heat transfer rates approximately 50% higher than for the infinite stream at $\phi = 0$.

The small effect of ℓ/b in Fig. 12 is consistent with the behavior pictured in Fig. 10. For a constant value of $N_{R,\ell}$, an increase in ℓ/b dictates a proportionate decrease in $N_{R,n}$, by virtue of (20). For example, an increase in ℓ/b from 3.125 to 6.25 at $N_{R,\ell} = 11{,}550$ is accompanied by a decrease in $N_{R,n}$ from 7400 to 3700. This results in a 6.5% increase in $N_{St,av}$ from 1.08×10^{-2} to about 1.15×10^{-2}. This effect decreases for increasing values of ℓ/b up to 12.5 where the converging nature of the curves of Fig. 10 begin to reverse the trend.

Effect of Nozzle Exit Velocity Profile

As mentioned earlier, the effect of the exit velocity profile is very small and for usual engineering purposes can be neglected. This conclusion was reached by repeating a number of the previously described tests with different exit profiles. As described in Appendix A, at a given nozzle Reynolds number, the velocity profile at the exit plane of the nozzle depends upon the ratio of throat length to hydraulic diameter in the nozzle. This velocity profile is characterized by the ratio of the centerline velocity at the nozzle exit to the average velocity at the exit plane, $u_{\text{¢}}/U$. The three geometrically similar nozzles shown in Fig. 6 were designed to have the same L/D_H and $u_{\text{¢}}/U$ at three different values of the nozzle spacing, b. Thus a particular test could be run three times with everything but the ratio $u_{\text{¢}}/U$ held constant by changing nozzles, but holding the nozzle spacing and flow rate constant.

Figure 13 shows the effect of the exit velocity profile on the $N_{St,av}/(N_{St,av})_{max}$ curves. Here two nozzles were used: one with a value of $u_{\text{¢}}/U \simeq 1.15$ and one with $u_{\text{¢}}/U \simeq 1.35$. For narrow nozzles with small aspect ratios

a value of $u_{\ell}/U = 1.35$ represents almost fully developed flow at the nozzle exit[11]. Thus it is felt that the nozzle exit profiles tested represent as wide a range of the profile as would be found in a design situation.

Figure 14 is a plot of the results of the same two nozzles compared for their effect on the $N_{St,av}$ vs. $N_{R,\ell}$ curves. This graph best indicates the small influence of the effect of the exit velocity profile. The heat transfer to the jet with the more uniform velocity profile is apparently less than that to the jet with the higher centerline velocity; which is expected, since the latter jet has associated with it a higher kinetic energy. However, the effect is sufficiently small for the two cases to be within the experimental uncertainty.

Local Heat Transfer Coefficients

The average heat transfer results, Fig. 10, have been used to calculate local heat transfer coefficients in the manner discussed previously (see Fig. 4 and the associated text) and are presented in Fig. 15.

Further Correlation of the Results

The analysis indicates that in the region near the stagnation point the local heat transfer should be related to the nozzle flow through (14); that is

$$N_{St}\, N_{R,n}{}^{1/2} = \text{constant}.$$

Using this prediction as an indication of the form to be expected, the entire results of Fig. 15 were correlated on the basis of $N_{St}(N_{R,n})^{p} = \text{constant}$. This correlation is shown in Fig. 16 with $p = 0.434$. It can be seen that the correlation is quite good even in the regions far away from the stagnation point.

Fig. 13

EFFECT OF NOZZLE EXIT VELOCITY PROFILE

ON $N_{St,av}/(N_{St,av})_{max}$

(See Table 10 for tabulated results)

$b = 0.020"$

$\ell/b = 12.5$

$N_{R,n} = 4500$

$\phi = 90°$

FIG. 14

EFFECT OF NOZZLE EXIT VELOCITY PROFILE

ON $N_{St,av}$ VERSUS $N_{R,\ell}$

(See Table 10 for tabulated results)

$b = 0.020$

$\ell/b = 25.0$

$\delta/b = 8.0$

$\phi = 90°$

FIG. 15

LOCAL HEAT TRANSFER, N_{St} VERSUS x/b

$\delta/b = 8.0 \quad \phi = 90°$

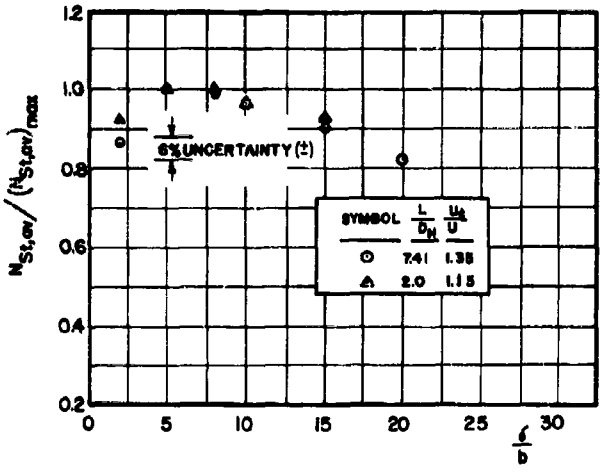

FIG. 13

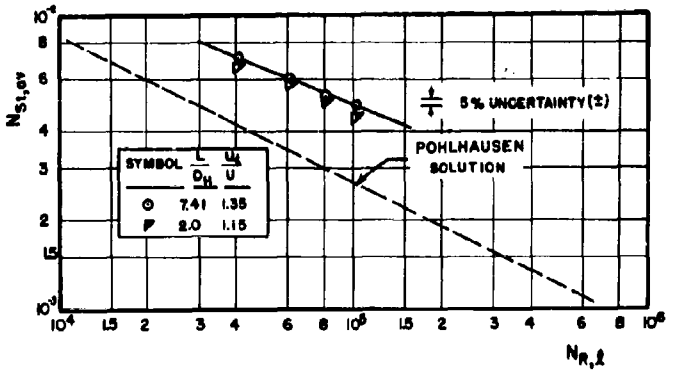

FIG. 14

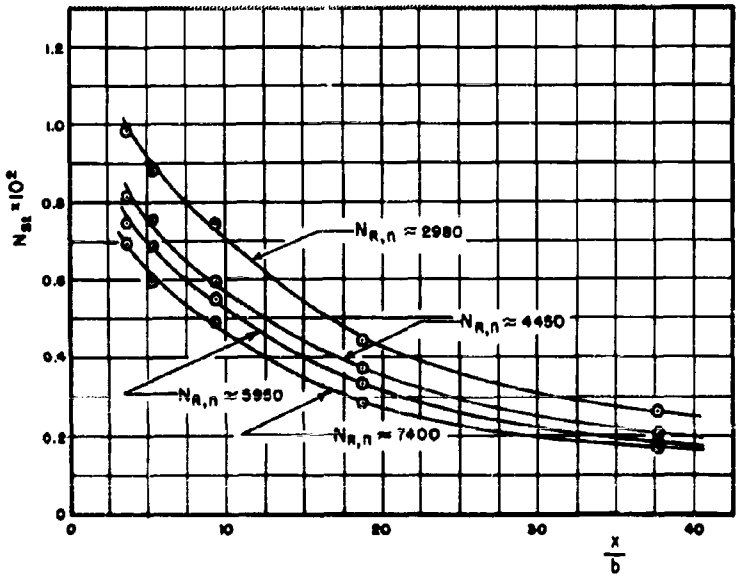

FIG. 15

This correlation can be extended still further. Figure 17 is a plot of the average heat transfer results treated in the same manner; that is, $N_{St,av} N_{R,n}^{0.434}$ as a function of ℓ/b . Again the correlation is good.

The exponent $p = 0.434$ was selected on the basis of the following considerations. The results were first correlated as indicated by the analysis with $p = 0.50$, and the correlation was reasonably satisfactory. However, it was noted in Eq. (20) that there is an approximate linear relationship between $N_{R,\ell}$ and $N_{R,n}$ and it can be observed that the results of $N_{St,av}$ vs. $N_{R,\ell}$ in Fig. 12 plot with a slope of -0.434 instead of -0.50. With $p = 0.434$ the correlation with $N_{R,n}$ is better than that obtained with $p = 0.50$.

It should be noted that the best interpretation line for the local heat transfer results, Fig. 16, is analytically related to the best interpretation line for the average results, Fig. 17, through Eq. (18). The best interpretation line on Fig. 16 was derived in this manner.

The dotted curves in Figs. 16 and 17 indicate qualitatively the probable behavior of the local and average heat transfer coefficients at and near the stagnation point. It should be noted that at the stagnation point the local and average heat transfer coefficients should be equal; thus a substantial rise in the local coefficient near this point is needed, as indicated in Fig. 16. Such behavior is in good agreement with the behavior of circular jets near the stagnation point.[1]

Effect of the Prandtl Number

Since air at approximately 530° R was the only fluid used in the tests ($N_{Pr} = 0.705$), the effect of N_{Pr} was not observed. However, the effect of this parameter is predicted analytically in (13).

$$N_{St}\, N_{R,n}^{0.5}\, N_{Pr}^{0.63} = \text{constant}$$

If the results of this investigation are used with other fluids, it is recommended that (13) be used as a guide in predicting the effect of N_{Pr}. This N_{Pr} effect is included in the equations below.

Experimental Results in Equation Form

The results presented in Fig. 12 are readily expressible in equation form. If the small effect of ℓ/b is regarded as a spread in the data, then the results may be characterized with a single line. When the effect of N_{Pr} suggested by (13) is included, the result is

$$N_{St,av}\, N_{R,\ell}^{0.434}\, N_{Pr}^{0.63} = 0.547 \pm 0.025 \qquad (22)$$

for $7 < \frac{\delta}{b} < 10$ and $3 < \frac{\ell}{b} < 50$.

Using the relation between $N_{R,\ell}$ and $N_{R,n}$ as given by (20), the above equation can be expressed as

$$N_{St,av}\, N_{R,n}^{0.434}\, N_{Pr}^{0.63} = 0.74 \left(\frac{\ell}{b}\right)^{-0.434} \qquad (23)$$

for $7 < \frac{\delta}{b} < 10$ and $3 < \frac{\ell}{b} < 50$. This equation is shown in Fig. 17.

FIG. 16

CORRELATED LOCAL HEAT TRANSFER RESULTS

$N_{St}\ N_{R,n}^{0.434}$ VERSUS x/b

($N_{Pr} = 0.705$)

The data points were obtained from Fig. 15
(See Fig. 4 and Appendix E for method)
The dotted curve was obtained from Fig. 17
in a similar manner.

FIG. 17

CORRELATED AVERAGE HEAT TRANSFER RESULTS

$N_{St,\ av}\ N_{R,n}^{0.434}$ VERSUS ℓ/b

($N_{Pr} = 0.705$)

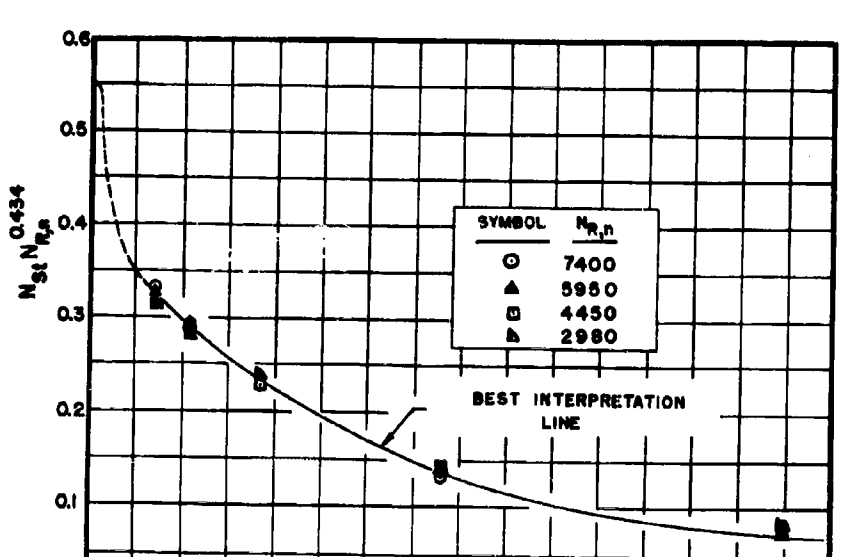
0.6
0.5
0.4
0.3
0.2
0.1
0
0
5
10
15
20
25
30
35
40
$N_{St} N_{R,n}^{0.434}$
SYMBOL
$N_{R,n}$
7400
5950
4450
2980
BEST INTERPRETATION LINE
$\frac{x}{b}$

FIG. 16

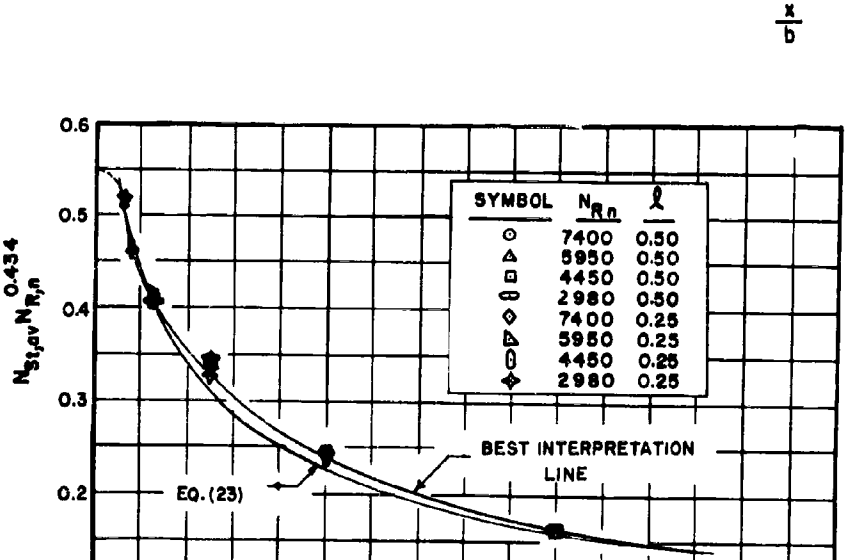
0.6
0.5
0.4
0.3
0.2
0.1
0
0
10
20
30
40
50
60
70
80
$N_{St,av} N_{R,n}^{0.434}$
SYMBOL
$N_{R,n}$
$\frac{l}{b}$
7400 0.50
5950 0.50
4450 0.50
2980 0.50
7400 0.25
5950 0.25
4450 0.25
2980 0.25
BEST INTERPRETATION LINE
EQ. (23)
$\frac{l}{b}$

FIG. 17

VII COMPARISON WITH CIRCULAR JETS

In order to gain some preliminary insight as to the relative performance of the slot jets and the more common circular jets, one circular nozzle and two circular targets were used. The nozzle was designed so as to be quite similar to the slot nozzles as regards discharge coefficient, L/D_H ratio, etc. The details of this nozzle, together with its discharge coefficient calibration, are included in Appendix A. The throat area of this nozzle and the throat area of the slot nozzles set at a thickness of 0.040 inch are identical; that is, $A = 0.030$ in.^{2} and thus the diameter is 0.196 inch. The two circular targets have diameters of 1.0 and 0.50 inch, respectively. The results obtainable with this equipment are restricted to the region near the stagnation point since the nozzle is relatively large compared to the target diameter.

The effect of nozzle-to-target distance, δ/D, was investigated with the circular jets, and the behavior was quite different than that obtained with the slot jets. Figure 18 shows the results of these tests. Data was taken at δ/D values of 1.0, 5.0, and 8.0, and the results indicate that the heat transfer drops off monotonically with increasing distance, δ/D. In order to be consistent with the slot jet tests, which were taken with a δ/D ratio which gave maximum heat transfer, the remaining tests for the circular jets were taken with $\delta/D = 1.0$, or $\delta = 0.196$ inch. Figure 19 presents the results of these tests. $N_{St,av}$ is given as a function of $N_{R,n}$ and ℓ/D, where ℓ is the radius of the target and D is the diameter of the nozzle. Figure 19 for the circular jets is thus analogous to Fig. 10 for the slot jets.

It is interesting to compare the circular jet on the basis of the correlating parameter, $N_{St,av} N_{R,n}^{0.434}$ which was found of use for the slot jets. In Fig. 20 the best

curve through the slot jet results of Fig. 17 is drawn together with the results of the circular jets. As can be seen, the circular jet results do not differ significantly from the slot jet behavior, at least in the narrow ℓ/D test range for the circular jets.

One of the tests for the circular jet (see Run number 508, Table 11) indicates that a flow rate of 11 pounds per hour (V_{jet} = 195 ft/sec) impinging on the one-inch diameter target results in an average Stanton number, $N_{St,av}$, of 7.24×10^{-3} and an h_{av} = 91.6 Btu/(hr °F ft^2) over the target surface. This particular target has an area of 0.785 in.^{2}. An interesting comparison may be drawn between this heat transfer and that obtainable with a slot jet cooling the same size area. To make a valid comparison, the flow rate and exit area of the slot nozzle should be the same as that of the circular one. This restriction insures that the compressor power required for the air supply will be identical for both nozzles. As has already been mentioned, the slot nozzle 0.750 inch wide and 0.040 inch thick has the same area as the circular nozzle. With these facts in mind, the results of Fig. 17 can be used to predict the corresponding slot jet heat transfer. Setting the two target areas equal:

$$0.785 = 0.750\ (2\ell)$$

therefore, ℓ = 0.522 inch and ℓ/b = 13

The nozzle Reynolds number may be computed from the flow rate and dimensions of the nozzle:

$$N_{R,n} = \frac{w/A \cdot D_H}{\mu} = \frac{2w}{\mu\ (b+c)} = 7670$$

At ℓ/b = 13, $N_{St,av}\ N_{R,n}^{0.434} = 0.325$ from Fig. 17.
Therefore, $N_{St,av} = 6.7 \times 10^{-3}$ (h_{av} = 84.7 Btu/(hr ft^2 °F)

and the circular jet yields an h_{av} approximately 8% higher than this particular slot jet while cooling the same area with the same flow rate and nozzle area. However, while equal in magnitude, the shape of the two areas cooled are quite different. In fact, the shape of the area cooled is important in the above comparison.

Suppose that the slot jet had been 1.0 inch wide and 0.030 inch thick. Then the ℓ/b required to cool 0.785 $in.^2$ would still be 13, but the Reynolds number would be reduced to 5870. For this case, $N_{St,av} = 7.30 \times 10^{-3}$ and the average heat transfer coefficients for the circular and slot jets are about the same at the common flow rate of 11 lbs/hr. A tentative conclusion seems to be that the shape of the area to be cooled is of primary importance in deciding which type of jet would be more economical of compressor power for a desired cooling rate.

FIG. 18

EFFECT OF ℓ/D On $N_{St,av}$ FOR CIRCULAR JETS

(See Table 11 for tabulated results)

$\phi = 90°$

FIG. 19

EFFECT OF ℓ/D ON $N_{St,av}$ FOR CIRCULAR JETS

AT CONSTANT $N_{R,n}$

(See Table 11 for tabulated results)

$\phi = 90°$

$\ell/D = 1.0$

FIG. 20

COMPARISON OF CIRCULAR AND SLOT JETS

$N_{St,av} N_{R,n}^{0.434}$ vs ℓ/b, ℓ/D

Data points are for the circular jets.

Solid curve is result of Fig. 17 for slot jets

$\phi = 90°$

$\ell/b = 8.0$ $\ell/D = 1.0$

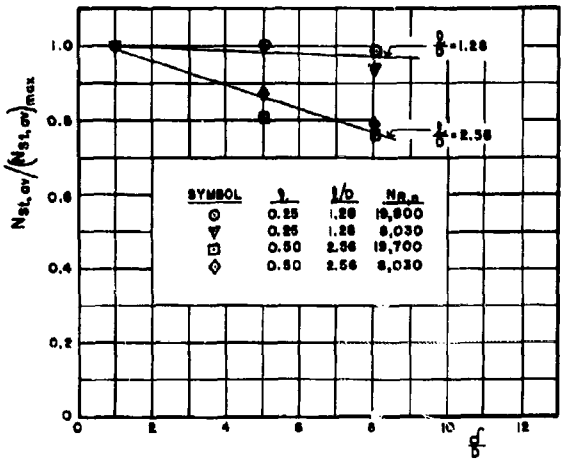

FIG. 18

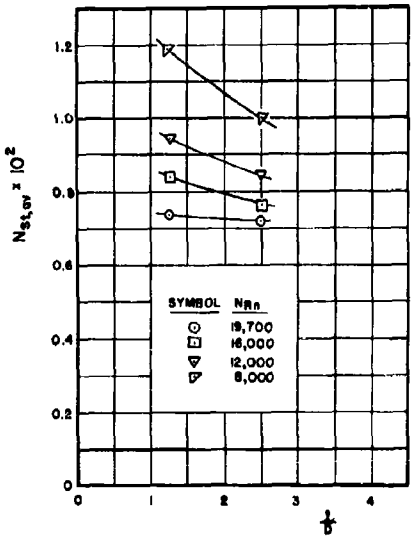

FIG. 19

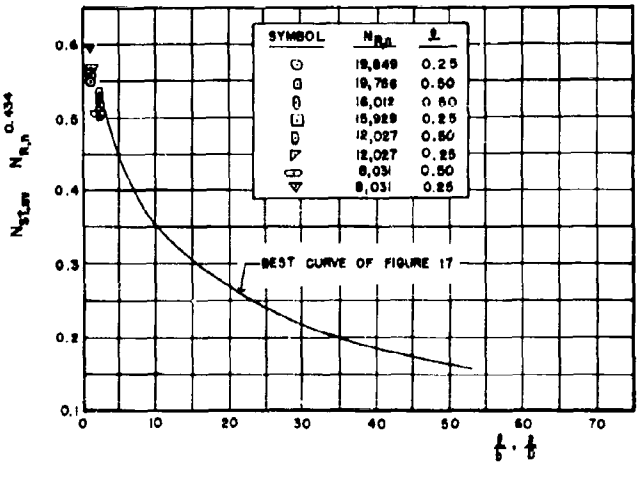

FIG. 20

VIII APPLICATION TO DESIGN

The foregoing comparison between circular and slot jets illustrates how heat transfer coefficients may be readily predicted for the slot jets by use of the results of Figs. 16 and 17. These results are, of course, valid only for nozzle-to-target distance in the range 7 to 10. Figure 9, however, should provide a qualitative appreciation for how these results are modified by changes in δ/b outside this range. Although the nozzle Reynolds numbers for the tests were fairly low, they are typical of a design situation where small nozzles are used for localized cooling or heating. The specific point of view taken in this study has been that the jet would be used for cooling a hot surface, but the results are equally applicable for heating a cool surface.

In applying the results of this study to a design it should be noted that the results are evaluated on the basis of a difference between the jet total (or stagnation) temperature and the target surface temperature. The jet static (or thermodynamic) temperature is lower than the total temperature by the kinetic energy effect of the jet, and this difference is proportional to the square of the velocity. In the present study, the plenum pressure was as high as 16 inches of mercury gage; and thus the maximum difference between the jet static and total temperatures amounted to about 20 degrees.

If the cooling, or heating, is to be done with arrays of jets rather than with one individual jet, interaction between the individual jets in the array must be recognized. The results here do not account for any interaction and are strictly applicable only to individual jets. Nevertheless, there are many configurations where arrays of slot jets may be used without appreciable interaction between them. For circular jets in arrays, interaction is always present and such interaction lowers the average heat transfer rates[1].

Thus, for certain applications of arrays of jets, the slot jet may have an advantage over the circular jet.

It should be noted that the magnitudes of the conductance, h, obtainable with impinging jets (50-250 Btu/hr ft^2 °F) are significantly higher than those normally encountered (10-50 Btu/hr ft^2 °F) in forced convection situations with air at approximately atmospheric density.

IX SUMMARY AND CONCLUSIONS

A transient technique for the experimental determination of impinging jet average heat transfer coefficients has been described, and the method has been extended to yield local heat transfer coefficients. The technique was used to investigate extensively the case of a slot jet impinging normally on a plane surface. The experimental data for this case is correlated on a dimensionless basis, Figs. 16 and 17, which makes extensions to other gases, nozzle dimensions, and target dimensions feasible. This greater generality is of importance to the designer.

The wedge solution (14) analysis indicated that the dimensionless parameter $N_{St}\, N_{R,n}^{p}$ should be useful in correlating local heat transfer data near the stagnation region. Indeed, this parameter proved valid for correlating not only these results but also local results away from the stagnation region and average heat transfer results as well. (See Figs. 16 and 17 and Eq. (23).)

The results were also presented on the basis of $N_{St,av}$ vs. $N_{R,\ell}$, Fig. 12. On this basis the effect of ℓ/b is minor and the results are readily represented by a single equation (22). In some respects Fig. 12 and Eq. (22) may prove to be the most convenient presentation of results from the point of view of the designer.

The transient technique was also used to experimentally investigate in a preliminary way the case of a normally impinging circular jet on a plane surface. This study was limited to only a few tests, and the results were used as a comparison with the slot jet results. It was tentatively concluded that the shape of the area to be cooled is of primary importance in deciding between a circular or slot jet. However, if arrays of jets are to be used, the slot jets may be more desirable since interaction between them can be held to a minimum.

X RECOMMENDATIONS FOR FURTHER WORK

The experimental apparatus and techniques now available can be used to extend the results of this study as follows:

(1) the circular jet impinging normally,
(2) the slot jet impinging at $0° \leq \phi < 90°$,
(3) the slot jet impinging on a cylindrical surface,
(4) more tests for the normally impinging slot jet to extend the Reynolds number and ℓ/b ranges,
(5) the circular and slot jets operating with higher plenum pressures to investigate supercritical jets and the influence of shock wave patterns on heat transfer.

In addition, it would be desirable to re-examine the analytic treatment of the problem with a view to extending this treatment away from the stagnation region and into the wall jet region.

APPENDIX A - DESIGN AND CALIBRATION OF THE FLOW NOZZLES

At the outset of this study, it was felt that the heat transfer coefficients obtained with the impinging jets might depend to some extent on the character of the nozzle exit plane velocity profile as well as the mean flow properties of the jet.

With this in mind, three geometrically similar nozzles were designed to operate with jet thicknesses of 0.020, 0.040, and 0.080 inch, respectively.

The reasoning behind the design is based on the following functional relationship for the nozzle discharge coefficient, C:

$$C = f\ (\text{nozzle contour},\ L/D_H\ ,\ N_{R,n}) \qquad (24)$$

This relationship has previously been substantiated both analytically and experimentally for circular nozzles with laminar flow[10]. It was felt that this relationship would be valid for slot nozzles as well as circular nozzles.

A design L/D_H ratio of 2.0 and an elliptical contour were chosen for the three nozzles, as shown in Fig. 21. The discharge coefficients for the completed nozzles were obtained by comparing the measured flow, w_m, through the rotameter with an ideal $(C = 1.0)$ one dimensional flow through the nozzle based on the temperature and pressure in the plenum chamber just upstream of the nozzle. That is:

$$w_i = 4070\ A\ Y_a\ \left(\frac{P_n\ \Delta P_n}{T}\right)^{1/2} \qquad (25)$$

where Y_a is the nozzle expansion factor for the perfect gas compressible fluid[9]. The discharge coefficient is thus:

$$C = \frac{w_m}{w_i} \qquad (26)$$

Figures 22, 23, and 24 present the calculated discharge coefficients for the three nozzles at various nozzle spacings; that is, at various L/D_H ratios. Figure 25 shows a correlation between the three nozzles when all are operated at their design configuration of $L/D_H = 2.0$. The correlation is compared with the analytical results of Ref. 10 for the circular nozzles at the same L/D_H ratio. From this comparison it is clear that the slot nozzles compare favorably on a D_H basis with the predictions for the circular nozzle. The three nozzles at values of L/D_H other than 2.0 also agree well with the results of Ref. 10.

The discharge coefficient, of course, does not furnish a complete description of the nozzle flow. What is needed beyond this is some knowledge of the velocity profile at the exit plane of the nozzle. Experimental determination of the profile, or even of the centerline velocity, is impractical in this case because of the small size of the nozzles. However, since the flow in the nozzles is laminar, the flow pattern may be estimated using theory developed for the laminar entry length problem in rectangular ducts. Han[11] has published an analysis of this problem in which he presents u_{ℓ}/U in the developing region for different aspect ratios from 1.0 to 0. Figures 22, 23, and 24 include values of u_{ℓ}/U computed from Ref. 11.

For the tests with circular jets, one circular nozzle was designed with the contour shown in Fig. 21. As mentioned previously, it was designed to have the same area as the slot nozzle set to a thickness of 0.040 inch. It has an L/D_H ratio of 1.55. Figure 26 is a plot of discharge coefficient versus nozzle Reynolds number for the nozzle.

Table 1 is a tabulation of the nozzle variables for both the circular and slot types.

TABLE 1

Nozzle Type	L (in.)	b (in.)	A (in.^{2})	D_H (in.)	L/D_H
0.020 slot	0.0780	0.010	0.0075	0.01975	3.95
		0.020	0.0150	0.0390	2.00
		0.040	0.0300	0.0760	1.025
		0.060	0.0450	0.1111	0.702
		0.080	0.0600	0.1445	0.540
0.040 slot	0.1520	0.010	0.0075	0.01975	7.70
		0.020	0.0150	0.0390	3.90
		0.040	0.0300	0.0760	2.00
		0.060	0.0450	0.1111	1.38
		0.080	0.0600	0.1445	1.05
0.080 slot	0.2890	0.010	0.0075	0.01975	14.6
		0.020	0.0150	0.0390	7.41
		0.040	0.0300	0.0760	3.8
		0.060	0.0450	0.1111	2.62
		0.080	0.0600	0.1445	2.0
		D (in.)			
Circular	0.304	0.196	0.0300	0.196	1.55

FIG. 21

NOZZLE CONTOURS

(2 x Full Scale)

SLOT NOZZLES

0.080 NOZZLE (L/D_H=2.0 WHEN b = 0.080 in.)

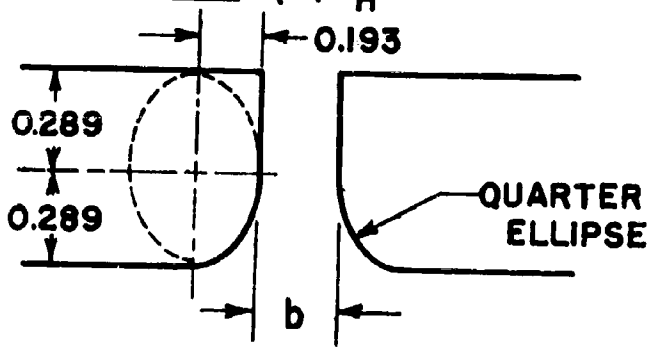

0.040 NOZZLE (L/D_H= 2.0 WHEN b = 0.040 in.)

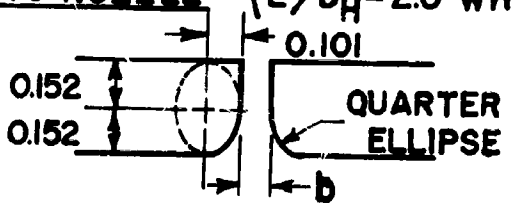

0.020 NOZZLE (L/D_H= 2.0 WHEN b = 0.020 in.)

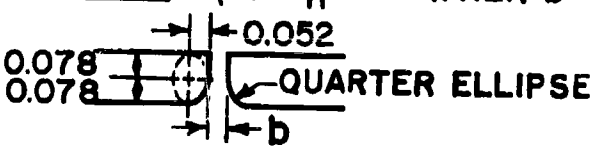

CIRCULAR NOZZLE

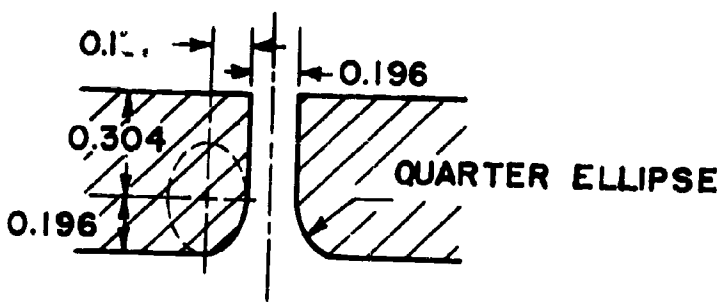

FIG. 21

FIG. 22

DISCHARGE COEFFICIENT FOR THE NOMINAL 0.020

SLOT NOZZLE

(L/D_H = 2.0 when b = 0.020 in.)

FIG. 23

DISCHARGE COEFFICIENT FOR THE NOMINAL 0.040

SLOT NOZZLE

(L/D_H = 2.0 when b = 0.040 in.)

FIG. 24

DISCHARGE COEFFICIENT FOR THE NOMINAL 0.080

SLOT NOZZLE

(L/D_H = 2.0 when b = 0.080 in.)

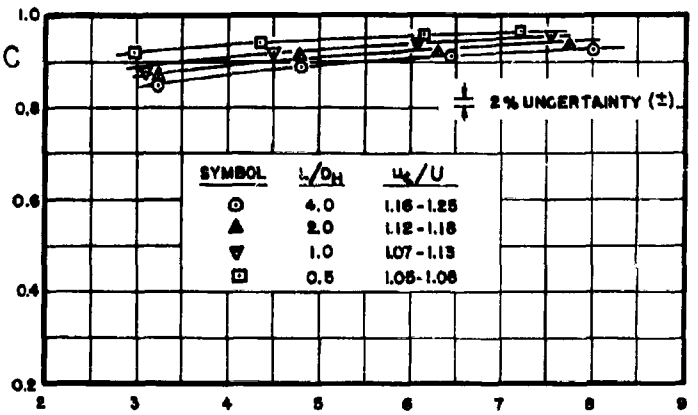

FIG. 22

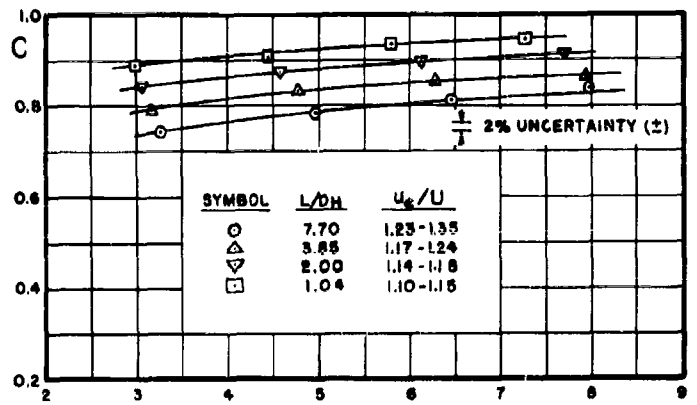

FIG. 23

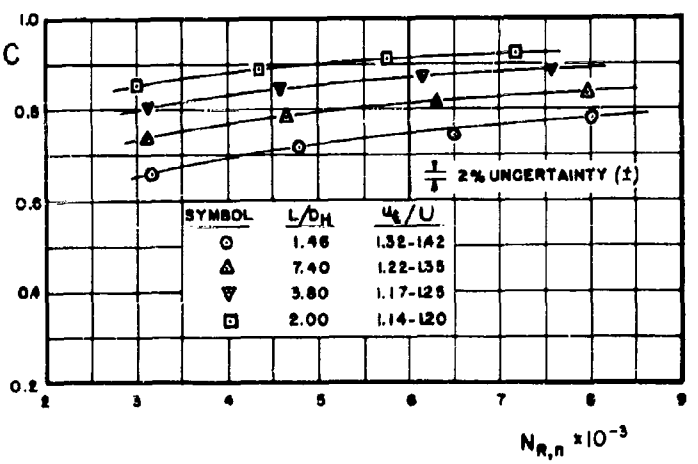

FIG. 24

FIG. 25

DISCHARGE COEFFICIENT FOR THE THREE SLOT NOZZLES

AT $L/D_H = 2.0$

The dotted curve is an analytical result

for $L/D_H = 2.0$ from Ref. 10

FIG. 26

CIRCULAR NOZZLE DISCHARGE COEFFICIENT

$L/D_H = 1.55$

FIG. 27

TARGET TEMPERATURE RESPONSE FOR RUN NO. 153

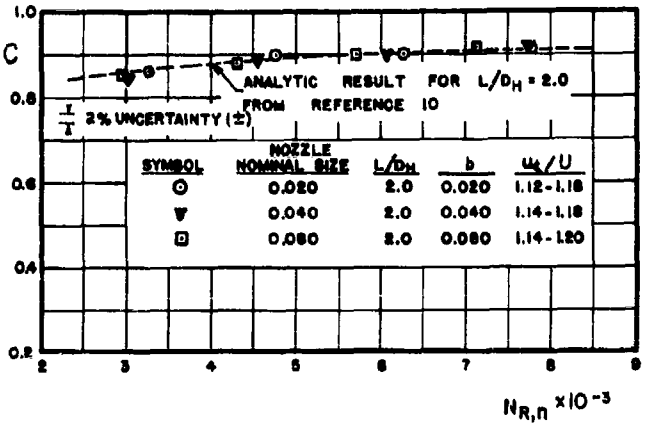

FIG. 25

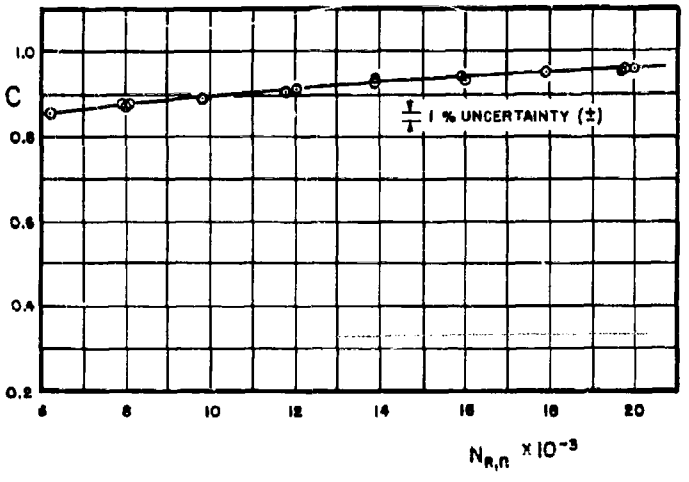

FIG. 26

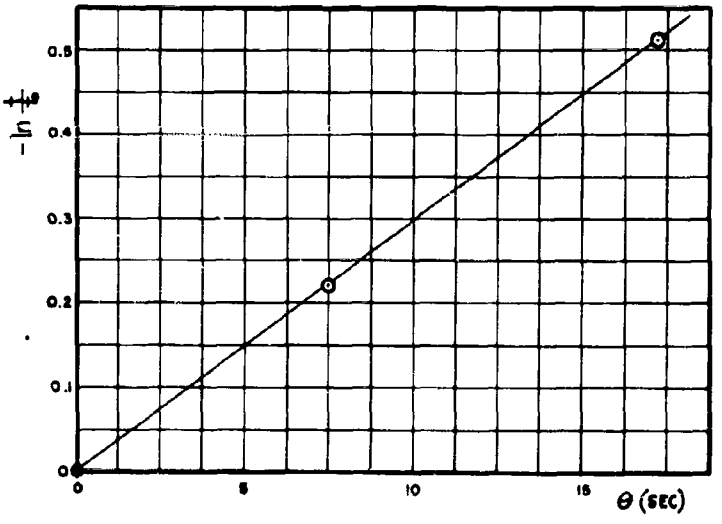

FIG. 27

APPENDIX B - CALIBRATION OF HEAT LEAK FROM TARGET

In the early stages of the project, it was found that the back side of the model could not be sufficiently insulated by simply imbedding it in a material of low thermal conductivity, such as balsa wood. When this was attempted, there appeared to be some initial heat leak into the balsa wood support combined with a subsequent feedback heat transfer from the support to the target during the transient test. The feedback effect appeared as a nonlinearity in the transient curve of θ versus $\ell n\ t/t_o$. To resolve this problem, it was decided to allow heat leak to occur only in one direction from the back side of the target, but in a manner such that it could be calibrated and allowed for in the analysis of the experimental results. Section III, Experimental Method, indicates how this leak may be accounted for in the analysis. [See Eq. (16)]

In order to calibrate the leak, the rear of the target was exposed to a cavity in the balsa wood support rather than being simply imbedded in the support. (See Fig. 3a). For calibration, the model was heated and then the target or front surface was covered with a matching balsa wood block and cavity. The free convection transient cooling was then recorded and a value of h_{leak} computed under the assumption that the average conductance, h_{av} , over the entire target would be equal to h_{leak} . This technique was used for all four models, two rectangular and two circular, used in the tests.

The results of this calibration are summarized below. The correction factor of Eq. (16), $h_{leak}\ (\frac{A_{leak}}{A_{forced}})$ is given for the four targets.

Note that the heat leak effect was generally less than 5% of the forced convection effect.

TABLE 2 - HEAT LEAK CORRECTION FACTORS

Target	Correction Factor $h_{leak} \frac{A_{leak}}{A_{forced}}$, $\frac{Btu}{hr\ ft^2\ °F}$	h_{leak}, $\frac{Btu}{hr\ ft^2\ °F}$
large rectangular (ℓ = 0.50 in.)	3.21	1.31
small rectangular (ℓ = 0.25 in.)	4.83	1.61
large circular (D = 1.0 in.)	2.08	1.04
small circular (D = 0.5 in.)	4.87	1.62

APPENCIX C - EXPERIMENTAL UNCERTAINTY

The experimental uncertainties were estimated for the results as follows:

TABLE 3 - SUMMARY OF UNCERTAINTIES

Quantity	Uncertainty
$N_{St,av}$	± 5%
$N_{St,av}/(N_{St,av})_{max}$	± 6%
C (slot nozzles)	± 2%
C (circular nozzle)	± 1%

No uncertainties were estimated for the local heat transfer results although they are certainly somewhat greater than 5%, since there are uncertainties in the graphical differentiating used to obtain them. This is particularly true in the region close to the stagnation point where the curvature of the $N_{St,av}$ versus ℓ/b results increases rapidly.

APPENDIX D - PHYSICAL PROPERTIES OF TARGETS

Altogether, four flat plate targets were used in the tests. Their physical properties, including dimensions, are summarized in Table 4 below.

TABLE 4 - TARGET PROPERTIES

Material (all targets): Commercial grade cast rolled copper

$$\text{specific heat} = 0.0923 \frac{\text{Btu}}{\text{lb}^{\circ}\text{F}}$$

Flat Plate Target	Weight	Dimensions	$\overline{C}/A_{forced}$
rectangular	17.15 grams	0.980"x0.500"x0.243	1.022 $\frac{\text{Btu}}{\text{ft}^2{}^{\circ}\text{F}}$
rectangular	8.78 grams	0.505"x0.490"x0.250"	1.035 $\frac{\text{Btu}}{\text{ft}^2{}^{\circ}\text{F}}$
circular	28.05 grams	1.0" diam x 0.250"	1.045 $\frac{\text{Btu}}{\text{ft}^2{}^{\circ}\text{F}}$
circular	7.22 grams	0.50" diam x 0.250"	1.08 $\frac{\text{Btu}}{\text{ft}^2{}^{\circ}\text{F}}$

APPENDIX E - DATA REDUCTION METHODS

Average Heat Transfer Coefficients

As an example of the data reduction method used to obtain the average coefficients, run number 153 will be reduced here. This is a slot nozzle test taken with the 0.080 nozzle set at a thickness of 0.040 inch. The jet emerging from this nozzle impinged on the small target (ℓ = 0.25 inch). The test data is given in Table 5 below.

TABLE 5 - TEST DATA FOR RUN NO. 153

Rotameter Pressure	66.85 in. Hg gage at 68° F
Rotameter Temperature	520.0° R
Rotameter Reading	95.2%
Dimensions:-	
δ	0.320 in.
b (See Fig. 1d)	0.040 in.
c (See Fig. 1d)	0.750 in.
ℓ (See Fig. 1d)	0.25 in.
Plenum gage pressure	9.63 in. H_2O at 68° F
Plenum temperature	520.0° R
Barometric pressure	30.00 in. Hg abs. at 32° F
θ at t = 2.50 millivolts	0.0 seconds
θ at t = 2.00 millivolts	7.5 seconds
θ at t = 1.50 millivolts	17.2 seconds

For the 0.080 nozzle, the throat length L equals 0.2890 inch, and when set at b = 0.040 inch the L/D_H ratio is 0.0760 (see Table 1). The measured flow rate through the rotameter is obtained from the equation:

$$w_m \left(\frac{lb}{hr}\right) = 0.0615 \text{ (Rotameter reading)} \frac{\left[\frac{\text{meter pressure (psia)}}{14.7}\right]^{1/2}}{\left[\frac{\text{meter temp. (°R)}}{530.0}\right]^{1/2}}$$

With the above test data, the value is:

$$w_m = 10.61 \text{ lb/hr}$$

The ideal (C = 1.0) flow rate through the nozzle is computed from Eq. (26):

$$w_i = 4070 \text{ A } (\text{in.}^2) \text{ } Y_a \left(\frac{P_n \Delta P_n}{T}\right)^{1/2}$$

where Y_a is obtained from Ref. 9 as a function of pressure ratio (Y_a equals 0.988 for this test). Then

$$w_i = 12.1 \text{ lb/hr}$$

The nozzle discharge coefficient is thus:

$$C = \frac{w_m}{w_i} = 0.878$$

This coefficient compares closely with the calibrated coefficient of Fig. 24; the comparison gives a check on several variables as follows. System air leaks, errors in reading the rotameter, and errors in setting the nozzle gap can all be detected by checking the discharge coefficient.

The actual transient temperature response is plotted before the data is reduced to insure that the response on a semi-log plot is linear as specified by the analysis. A nonlinear response may indicate some aberation of the temperature-time measurements or that the one lump of thermal capacitance and resistance assumed in the analysis is invalid. The response for run number 153 is plotted in Fig. 27.

The heat transfer coefficient, h_{av}, is evaluated from Eq. (16):

$$h_{av} = - \left(\frac{\overline{C}}{A_{forced}}\right) \left(\frac{\ell n\ t/t_o}{\theta}\right) - h_{leak} \left(\frac{A_{leak}}{A_{forced}}\right)$$

where the constants, $\frac{\overline{C}}{A_{forced}}$ and $h_{leak} \left(\frac{A_{leak}}{A_{forced}}\right)$ are obtained from Tables 4 and 2 respectively. Thus:

$$h_{av} = - 1.035 \frac{\ell n\ (t/t_o)}{\theta(hr)} - 4.83 \frac{Btu}{hr\ ft^2\ °F}$$

From Fig. 27, $\theta = 17.2$ seconds when $\ell n\ t/t_o = - 0.512$ and this gives:

$$h_{av} = 106.2 \frac{Btu}{hr\ ft^2\ °F}$$

From Table 1, the throat area of the nozzle is 0.030 $in.^2$ and thus:

$$G = \frac{w_m}{A} = 50{,}941 \frac{lb}{hr\ ft^2}$$

From these results, $N_{St,av}$, $N_{R,n}$, and $N_{R,\ell}$ can be computed.

$$N_{St,av} = \frac{h_{av}}{Gc_p} = 8.695 \cdot 10^{-3}$$

$$N_{R,n} = \frac{D_H G}{\mu} = 7{,}400$$

$$N_{R,\ell} = \frac{\ell G}{\mu} = 24,341$$

where $\mu = 12.1 \times 10^{-6}$ lb/(ft sec) and $c_p = 0.239$ Btu/(lb °F) as obtained from Ref. 12.

The result of this test is plotted in Fig. 10 at $\ell/b = 6.25$.

Local Heat Transfer Coefficients

The subsequent test, run number 154, was taken at the same value of $N_{R,n}$ as 153, but with a ℓ/b ratio of 12.5. This run is also plotted in Fig. 10. For run number 154, $N_{St,av} = 6.752 \times 10^{-3}$ at $\ell/b = 12.5$. These two runs can thus be used to calculate the local heat transfer coefficients in the region between $\ell/b = 6.25$ and $\ell/b = 12.5$ as discussed in the section on Extension of the Transient Technique.

In the reduction of the data, N_{St} , the local heat transfer, was evaluated only at the midpoints between the average data. For example, runs 153 and 154 were used (actually, the curve faired through these and other runs at $N_{R,n} = 7400$ was used) to evaluate N_{St} at $x/b = 9.375$. For this evaluation Eq. (18) becomes:

$$(N_{St})_{x/b=9.375} = (N_{St,av})_{x/b=9.375} + 9.375 \left(\frac{d\ N_{St,av}}{dx}\right)_{x/b=9.375}$$

From Fig. 10, $(N_{St,av})_{x/b=9.375} = 7.60 \times 10^{-3}$ and the derivative is evaluated by taking the slope of the chord between the two values of $N_{St,av}$ at ℓ/b of 6.25 and 12.5. That is, $\Delta(N_{St,\ell/b}) = 1.80 \times 10^{-3}$ and $\Delta(\ell/b) = 6.25$. Thus

$$\left(\frac{d\ N_{St,av}}{dx}\right) \simeq \frac{-1.80 \times 10^{-3}}{6.25} = -2.88 \times 10^{-4}$$

The final result is $(N_{St})_{x/b=9.375} = 4.90 \times 10^{-3}$ and this is the value that is plotted in Fig. 15. Recall that these results are all for a constant value of $N_{R,n} = 7400$.

Machine Reduction of Data

The average heat transfer results were calculated on the Burroughs 220 digital computer located in the Stanford Computing Facility. The language used by the machine is the Balgol language. The following table gives translation from some of the nomenclature used in this paper to that used by the machine.

TABLE 6 - MACHINE LANGUAGE NOMENCLATURE

Quantity	Machine Equivalent
run number	R
nozzle to plate distance, δ	DELTA
nozzle spacing, b	BETA
transient time, θ	THETA
nozzle throat length, L	L
hydraulic diameter, D_H	DH
1/2 plate length, ℓ	LL
measured flow rate, w_m	W
ideal flow rate, w_i	WI
nozzle discharge coeff., C	C
conductance, h	H
$N_{R,\ell}$	REYLEN
$N_{R,n}$	REYNOZ
$N_{St,av}$	STANTON

The following page is a sample program as used to reduce run number 153 on the machine.

```
2 S441          JOB  1/16/62,    2MIN   D E METZGER  EXT 2176          .
2               LODX BALGOL                                            .
2 COMMENT  IMPINGING JET DATA REDUCTION PROGRAM FOR AVERAGE HEAT TRANSFER.1
2          COEFFICIENTS$                                               .2
2 INTEGER R$                                                           .3
2 INPUT DATA (R,MP,MT,MR,DELTA,BETA,DELTAPM,DELTAPW,BP,NT,THETA,L,DH)$  .4
2 FORMAT HEAD1(B1,*RUN*,B3,*LENGTH-WIDTH RATIO*,B3,*DISTANCE-WIDTH RATIO*,5
2              ,B3,*EXPAN-COEF,YA*,B6,*FLOW,LB/HR*,B5,*FLOW,LB/HRSQFT*,B3,6
2              ,*H,BTU/HRSQFTOF*,W0)$                                  .7
2 FORMAT HEAD2(B9,*L/DH*,B11,*NOZZLE COEF*,B7,*NOZ REYNOLDS NO*,B3,     .8
2              *PLATE REYNOLDS NO*,B2,*STANTON NO,H/GCP*,B4,            .9
2              *NUSSELT NO,HDH/K*,W2)$                                 .10
2 WRITE ($$HEAD1)$   WRITE ($$HEAD2)$                                  .11
2 LL=0.25$ CONST1=1910.0$ CONST2=4.83$ CP=0.2398$ K=0.0151$ MU=0.0436$ .12
2 START..READ($$DATA)$                                                 .13
2    W=0.0615(MR). SQRT((((MP+BP)(0.4893))/14.7)/(MT/530.0))$          .14
2    EITHER IF DELTAPM EQL 0.0$     PSIG=DELTAPW.(0.03605)$            .15
2    OTHERWISE$ PSIG=DELTAPM.(0.4893)$                                 .16
2    PATM=BP.(0.4893)$                                                 .17
2    PNOZ=PATM+PSIG$                                                   .18
2    YA=SQRT(((PATM/PNOZ)*1.43)(3.5)(1.0-(PATM/PNOZ)*0.286)/(1.0-(PATM .19
2       /PNOZ)))$                                                      .20
2    W1=4070.0(BETA)(0.750)(YA).SQRT(PNOZ.PSIG/NT)$                    .21
2    C=W/W1$                                                           .22
2    H=(CONST1/THETA)-CONST2$                                          .23
2    G=(144.0(W))/(0.750BETA)$                                         .24
2    REYLEN=(LL.G)/(12.0MU)$                                           .25
2    REYNOZ=(DH.G)/(12.0MU)$                                           .26
2    STANTON=H/(G.CP)$                                                 .27
2    NUSSELT=(H.DH)/(12.0K)$                                           .28
2       OUTPUT O1(R,LL/BETA,DELTA/BETA,YA,W,G,H)$                      .29

2       OUTPUT O2(L/DH,C,REYNOZ,REYLEN,STANTON,NUSSELT)$               .30
2       FORMAT F1(I5,6F19.8,W0)$                                       .31
2       FORMAT F2(B5,F14.8,5F19.8,W2)$                                 .32
2    WRITE ($$O1,F1)$  WRITE ($$O2,F2)$                                .33
2    GO TO START$                                                      .34
2    FINISH$                                                           .35
```

APPENDIX F - TABULAR RESULTS

Tables 7 to 10 summarize the reduced heat transfer data for slot jets and Table 11 summarizes the heat transfer data for circular jets.

Table 7 presents the effect of δ/b on $N_{St,av}$

Table 8 presents the effect of ℓ/b on $N_{St,av}$

Table 9 presents the effect of δ/b on $N_{St,av}$ vs ℓ/b

Table 10 presents the effect of nozzle exit velocity profile

Table 11 presents the circular jet results

TABLE 7. RESULTS OF EFFECT OF δ/b ON $N_{St,av}$ (SEE FIG. 9).

Run	P_n/P_a	w	G	b	ℓ/b	δ/b	$N_{R,n}$	$N_{R,\ell}$	$N_{St,av}$	h_{av}
ℓ = 0.25										
1	1.006	10.96	26,322	0.080	3.125	2.0	7269	12,577	0.00827	52.2
2	1.006	10.95	26,286	0.080	3.125	5.0	7260	12,561	0.00914	57.6
3	1.006	10.88	26,128	0.080	3.125	8.0	7216	12,485	0.0108	67.8
4	1.006	10.87	26,100	0.080	3.125	10.0	7208	12,471	0.0106	66.4
5	1.006	10.89	26,155	0.080	3.125	15.0	7224	12,498	0.00918	57.6
6	1.025	10.96	52,615	0.040	6.25	2.0	7643	25,141	0.00711	89.7
7	1.025	10.94	52,546	0.040	6.25	5.0	7633	25,108	0.00799	100.7
8	1.025	10.93	52,490	0.040	6.25	8.0	7625	25,081	0.00829	104.3
9	1.025	10.92	52,448	0.040	6.25	10.0	7619	25,061	0.00866	108.9
10	1.025	10.97	52,685	0.040	6.25	15.0	7653	25,174	0.00757	95.7
11	1.025	10.95	52,587	0.040	6.25	20.0	7639	25,128	0.00666	84.0
13	1.111	10.85	104,233	0.020	12.5	2.0	7770	49,805	0.00617	154.3
14	1.113	10.93	104,926	0.020	12.5	5.0	7821	50,136	0.00711	178.8
15	1.112	10.89	104,510	0.020	12.5	8.0	7790	49,938	0.00674	168.8
16	1.112	10.89	104,538	0.020	12.5	10.0	7792	49,951	0.00661	165.7
17	1.111	10.87	104,316	0.020	12.5	15.0	7776	49,845	0.00607	151.7
18	1.111	10.85	104,205	0.020	12.5	20.0	7768	49,792	0.00547	136.7
20	1.537	10.91	209,572	0.010	25.0	2.0	7911	100,140	0.00504	253.3
21	1.537	10.91	209,463	0.010	25.0	5.0	7907	100,087	0.00534	268.0
22	1.536	10.90	209,353	0.010	25.0	8.0	7903	100,035	0.00512	256.8
23	1.534	10.90	209,189	0.010	25.0	10.0	7897	99,956	0.00491	246.5
24	1.536	10.90	209,353	0.010	25.0	15.0	7903	100,035	0.00449	225.3
25	1.542	10.94	210,011	0.010	25.0	20.0	7929	100,349	0.00398	200.5
28	1.002	6.68	16,026	0.080	3.125	2.0	4426	7,658	0.0108	41.4
29	1.002	6.68	16,022	0.080	3.125	5.0	4425	7,656	0.0111	42.7
30	1.002	6.68	16,022	0.080	3.125	8.0	4425	7,656	0.0132	50.7
31	1.002	6.67	16,018	0.080	3.125	10.0	4424	7,654	0.0135	51.8
32	1.002	6.67	16,014	0.080	3.125	15.0	4423	7,652	0.0119	45.7
33	1.002	6.67	16,014	0.080	3.125	20.0	4423	7,652	0.0105	40.2
34	1.010	6.67	32,028	0.040	6.25	2.0	4652	15,304	0.00948	72.8
35	1.010	6.67	32,016	0.040	6.25	5.0	4651	15,300	0.00965	74.1
36	1.010	6.67	32,019	0.040	6.25	8.0	4651	15,298	0.0103	78.9
37	1.010	6.67	32,011	0.040	6.25	10.0	4650	15,296	0.0104	80.1
38	1.010	6.67	32,011	0.040	6.25	15.0	4650	15,296	0.00953	73.1
39	1.010	6.67	32,011	0.040	6.25	20.0	4650	15,296	0.00845	64.9
40	1.045	6.68	64,138	0.020	12.5	2.0	4781	30,647	0.00726	111.6
41	1.045	6.67	64,022	0.020	12.5	5.0	4772	30,592	0.00839	128.7
42	1.045	6.67	64,022	0.020	12.5	8.0	4772	30,592	0.00832	127.8
43	1.045	6.67	63,999	0.020	12.5	10.0	4771	30,581	0.00809	124.2
44	1.045	6.67	63,989	0.020	12.5	15.0	4770	30,576	0.00756	116.1
45	1.045	6.67	63,989	0.020	12.5	20.0	4770	30,576	0.00692	106.2
46	1.272	6.67	128,078	0.010	25.0	2.0	4835	61,199	0.00600	184.3
47	1.272	6.66	127,945	0.010	25.0	5.0	4830	61,136	0.00633	194.1
48	1.270	6.66	127,911	0.010	25.0	8.0	4828	61,120	0.00647	198.4
49	1.269	6.66	127,911	0.010	25.0	10.0	4828	61,120	0.00613	188.1
50	1.269	6.66	127,878	0.010	25.0	15.0	4827	61,104	0.00577	177.1
51	1.269	6.66	127,865	0.010	25.0	20.0	4827	61,097	0.00512	157.0
77	1.001	4.51	10,824	0.080	3.125	2.0	2990	5,172	0.0135	35.0
78	1.001	4.51	10,827	0.080	3.125	5.0	2990	5,174	0.0139	36.1
79	1.001	4.50	10,808	0.080	3.125	8.0	2985	5,165	0.0158	40.9
80	1.001	4.50	10,792	0.080	3.125	10.0	2980	5,157	0.0166	42.9
81	1.001	4.49	10,781	0.080	3.125	15.0	2977	5,151	0.0149	38.5
ℓ = 0.50										
87	1.127	4.44	85,220	0.010	50.0	2.0	3217	81,441	0.00460	94.0
88	1.127	4.43	85,111	0.010	50.0	5.0	3213	81,337	0.00486	99.2
89	1.127	4.44	85,242	0.010	50.0	8.0	3218	81,462	0.00508	103.9
90	1.127	4.45	85,373	0.010	50.0	10.0	3223	81,588	0.00496	101.5
91	1.127	4.44	85,242	0.010	50.0	15.0	3218	81,462	0.00475	97.1
92	1 127	4.44	85,154	0.010	50.0	20.0	3214	81,379	0.00450	92.0
93	1.583	11.06	212,447	0.010	50.0	2.0	8020	203,027	0.00336	171.3
94	1.583	11.06	212,447	0.010	50.0	5.0	8020	203,027	0.00336	171.3
95	1.583	11.04	212,007	0.010	50.0	8.0	8003	202,606	0.00331	168.2
96	1.583	11.03	211,787	0.010	50.0	10.0	7995	202,396	0.00319	162.1
97	1.583	11.03	211,787	0.010	50.0	15.0	7995	202,396	0.00308	156.5
98	1.583	11.03	211,787	0.010	50.0	20.0	7995	202,396	0.00288	146.4

TABLE 8. RESULTS OF EFFECT OF ℓ/b ON $N_{St,av}$ (SEE FIG. 10).

Run	P_n/P_a	w	G	b	ℓ	ℓ/b	$N_{R,n}$	$N_{R,\ell}$	$N_{St,av}$	h_{av}
$\delta/b = 8.0$										
124	1.006	11.18	26,820	0.080	0.50	6.25	7407	25,631	0.00849	54.6
128	1.024	10.65	51,118	0.040	0.50	12.50	7425	48,852	0.00696	85.2
132	1.102	10.40	99,874	0.020	0.50	25.0	7445	95,445	0.00504	120.8
136	1.435	10.25	196,841	0.010	0.50	50.0	7430	188,113	0.00305	160.7
139	1.004	8.96	21,520	0.080	0.50	6.25	5943	20,565	0.00952	49.2
140	1.017	8.54	40,974	0.040	0.50	12.50	5951	39,157	0.00770	75.6
141	1.068	8.31	79,756	0.020	0.50	25.0	5945	76,219	0.00563	107.6
142	1.318	8.19	157,281	0.010	0.50	50.0	5937	15,031	0.00373	140.7
143	1.002	6.74	16,164	0.080	0.50	6.25	4464	15,448	0.0108	41.8
144	1.010	6.41	30,750	0.040	0.50	12.50	4467	29,387	0.00853	62.9
145	1.043	6.25	59,993	0.020	0.50	25.0	4472	57,333	0.00626	90.1
146	1.195	6.15	117,987	0.010	0.50	50.0	4454	112,755	0.00421	119.2
147	1.001	4.49	10,782	0.080	0.50	6.25	2978	10,304	0.0129	33.3
148	1.005	4.28	20,539	0.040	0.50	12.50	2984	19,628	0.0101	49.9
149	1.019	4.17	40,010	0.020	0.50	25.0	2982	38,236	0.00740	71.0
150	1.100	4.11	78,922	0.010	0.50	50.0	2979	75,423	0.00513	97.1
151	1.006	11.16	26,775	0.080	0.25	3.125	7395	12,794	0.0108	69.2
152	1.010	10.91	34,916	0.060	0.25	4.167	7414	16,684	0.00984	82.4
153	1.024	10.61	50,941	0.040	0.25	6.25	7400	24,341	0.00870	106.2
154	1.100	10.37	99,595	0.020	0.25	12.50	7424	47,590	0.00675	161.3
155	1.432	10.22	196,312	0.010	0.25	25.0	7410	93,803	0.00485	228.1
156	1.004	8.95	21,476	0.080	0.25	3.125	5931	10,262	0.0120	62.0
157	1.007	8.72	27,918	0.060	0.25	4.167	5928	13,340	0.0108	72.5
158	1.016	8.53	40,921	0.040	0.25	6.25	5944	19,553	0.00959	94.1
159	1.068	8.31	79,756	0.020	0.25	12.5	5945	38,110	0.00749	143.2
160	1.292	8.20	157,362	0.010	0.25	25.0	5940	75,192	0.00537	202.8
161	1.002	6.72	16,123	0.080	0.25	3.125	4453	7,704	0.0135	52.2
162	1.004	6.55	20,965	0.060	0.25	4.167	4452	10,018	0.0122	61.5
163	1.010	6.40	30,711	0.040	0.25	6.25	4461	14,675	0.0109	80.1
164	1.042	6.24	59,932	0.020	0.25	12.5	4467	28,637	0.00841	120.8
165	1.178	6.14	117,927	0.010	0.25	25.0	4452	56,349	0.00608	172.0
166	1.001	4.49	10,765	0.080	0.25	3.125	2974	5,144	0.0163	42.1
169	1.019	4.16	39,959	0.020	0.25	12.5	2979	19,094	0.00993	95.2
170	1.092	4.11	78,962	0.010	0.25	25.0	2981	37,730	0.00744	141.0
186	1.002	4.39	14,054	0.060	0.25	4.167	2984	6,716	0.0145	48.8
187	1.005	4.27	20,511	0.040	0.25	6.25	2979	9,801	0.0129	63.4

TABLE 9. RESULTS OF EFFECT OF δ/b ON $N_{St,av}$ VS ℓ/b (SEE FIG. 11).

Run	P_n/P_a	w	G	b	ℓ/b	δ/b	$N_{R,n}$	$N_{R,\ell}$	$N_{St,av}$	h_{av}
$\ell = 0.50$										
122	1.006	11.19	26,848	0.080	6.25	2.0	7415	25,657	0.00737	47.5
123	1.006	11.19	26,834	0.080	6.25	5.0	7411	25,644	0.00782	50.3
125	1.006	11.19	26,848	0.080	6.25	15.0	7415	25,657	0.00746	48.0
126	1.024	10.65	51,118	0.040	12.5	2.0	7425	48,852	0.00682	83.7
127	1.024	10.65	51,092	0.040	12.5	5.0	7422	48,827	0.00676	82.9
129	1.024	10.67	51,197	0.040	12.5	15.0	7437	48,926	0.00598	73.4
130	1.102	10.40	99,823	0.020	25.0	2.0	7441	95,397	0.00505	120.8
131	1.102	10.39	99,772	0.020	25.0	5.0	7437	95,348	0.00519	124.2
133	1.102	10.42	100,027	0.020	25.0	15.0	7456	95,591	0.00454	109.0
134	1.435	10.26	196,942	0.010	50.0	2.0	7434	188,209	0.00350	165.1
135	1.435	10.25	196,841	0.010	50.0	5.0	7430	188,113	0.00340	160.7
137	1.435	10.26	197,042	0.010	50.0	15.0	7438	188,305	0.00320	151.3
$\ell = 0.25$										
171	1.006	11.16	26,789	0.080	3.125	2.0	7399	12,801	0.00837	53.8
172	1.010	10.89	34,844	0.060	4.167	2.0	7399	16,649	0.00780	65.1
173	1.024	10.64	51,086	0.040	6.25	2.0	7421	24,410	0.00777	95.2
174	1.098	10.36	99,493	0.020	12.5	2.0	7416	47,541	0.00664	158.4
175	1.430	10.22	196,312	0.010	25.0	2.0	7410	93,803	0.00510	240.0
176	1.006	11.16	26,775	0.080	3.125	5.0	7395	12,794	0.00958	61.5
177	1.010	10.89	34,844	0.060	4.167	5.0	7399	16,649	0.00883	73.8
178	1.024	10.65	51,112	0.040	6.25	5.0	7424	24,423	0.00789	96.8
179	1.098	10.36	99,493	0.020	12.5	5.0	7416	47,541	0.00708	168.8
180	1.430	10.22	196,312	0.010	25.0	5.0	7410	93,803	0.00503	236.9
181	1.006	11.16	26,775	0.080	3.125	15.0	7395	12,794	0.00900	57.8
182	1.010	10.89	34,844	0.060	4.167	15.0	7399	16,649	0.00821	68.6
183	1.024	10.64	51,072	0.040	6.25	15.0	7419	24,404	0.00756	92.6
184	1.098	10.36	99,442	0.020	12.5	15.0	7413	47,516	0.00587	139.9
185	1.430	10.23	196,413	0.010	25.0	15.0	7414	93,852	0.00417	196.2

TABLE 10. RESULTS OF EFFECT OF NOZZLE EXIT VELOCITY PROFILE (SEE FIGS. 13 AND 14).

Run	P_n/P_a	w	G	δ/b	$N_{R,n}$	$N_{R,\ell}$	$N_{St,av}$	L/D_H
ℓ = 0.25, b = 0.020, ℓ/b = 12.5								
40	1.045	6.68	64,138	2.0	4781	30,647	0.00726	7.41
41	1.045	6.67	64,022	5.0	4772	30,592	0.00839	7.41
42	1.045	6.67	64,022	8.0	4772	30,592	0.00832	7.41
43	1.045	6.67	63,999	10.0	4771	30,581	0.00809	7.41
44	1.045	6.67	63,989	15.0	4770	30,576	0.00756	7.41
45	1.045	6.67	63,989	20.0	4770	30,576	0.00692	7.41
52	1.040	6.70	64,288	2.0	4792	30,718	0.00743	2.0
53	1.040	6.70	64,321	5.0	4795	30,734	0.00811	2.0
54	1.040	6.70	64,354	8.0	4797	30,750	0.00811	2.0
55	1.040	6.70	64,354	10.0	4797	30,750	0.00783	2.0
56	1.040	6.71	64,387	15.0	4799	30,766	0.00752	2.0
57	1.040	6.70	64,403	20.0	4801	30,774	0.00664	2.0
ℓ = 0.50, b = 0.020, ℓ/b = 25.0								
101	1.115	11.08	106,333	8.0	7926	101,618	0.00494	7.41
102	1.078	8.87	85,176	8.0	6349	81,399	0.00534	7.41
103	1.047	6.67	63,997	8.0	4770	61,159	0.00612	7.41
104	1.022	4.46	42,774	8.0	3188	40,877	0.00725	7.41
113	1.103	11.02	105,838	8.0	7889	101,145	0.00452	2.0
114	1.067	8.90	85,417	8.0	6367	81,630	0.00513	2.0
115	1.038	6.66	63,964	8.0	4768	61,128	0.00584	2.0
116	1.018	4.45	42,709	8.0	3184	40,815	0.00668	2.0

TABLE 11. CIRCULAR JET RESULTS (SEE FIGS. 18 AND 19).

Run	P_n/P_a	w	G	δ/D	$N_{R,n}$	$N_{St,av}$	h_{av}
ℓ = 0.50, D = 0.196, ℓ/D = 2.55							
508	1.021	11.05	52,762	1.0	19,766	0.00724	91.6
509	1.021	11.03	52,651	5.0	19,724	0.00585	73.9
510	1.021	11.05	52,762	8.0	19,766	0.00549	69.4
511	1.004	4.49	21,437	1.0	8,031	0.0100	51.5
512	1.004	4.49	21,448	5.0	8,035	0.00870	44.7
513	1.004	4.49	21,426	8.0	8,027	0.00787	40.4
514	1.015	8.95	42,742	1.0	16,012	0.00778	79.7
515	1.009	6.72	32,106	1.0	12,027	0.00856	65.9
ℓ = 0.25, D = 0.196, ℓ/D = 1.28							
516	1.022	11.10	52,985	1.0	19,850	0.00745	94.6
517	1.022	11.09	52,901	5.0	19,818	0.00747	94.6
518	1.022	11.04	52,706	8.0	19,745	0.00733	92.7
519	1.004	4.49	21,437	1.0	8,031	0.0119	61.5
520	1.004	4.49	21,426	5.0	8,027	0.0119	61.5
521	1.004	4.48	21,415	8.0	8,022	0.0111	57.1
522	1.014	8.90	42,521	1.0	15,929	0.00839	85.6
523	1.009	6.72	32,106	1.0	12,027	0.00950	73.2

TECHNICAL REPORTS DISTRIBUTION LIST, CONTRACT Nonr 225(23)

Chief of Naval Research
Department of the Navy
Washington 25, D. C.
(2)Attn: Code 429
(1) Code 438

(2)Commanding Officer
Office of Naval Research
Branch Office
1000 Geary Street
San Francisco 9, Calif.

(1)Commanding Officer
Office of Naval Research
Branch Office
1030 E. Green Street
Pasadena 1, Calif.

(1)Commanding Officer
Office of Naval Research
Branch Office
John Crerar Library Bldg.
86 E. Randolph Street
Chicago 1, Illinois

(25)Commanding Officer
Office of Naval Research
Branch Office
Keysign House
429 Oxford Street
London, W. I., ENGLAND
SEND TO:
Commanding Officer
Office of Naval Research
Branch Office
Navy No. 100
Fleet Post Office
New York, New York

Office of Naval Research
346 Broadway
New York 13, New York
(1)Attn: Dr. Saul Berman

Chief, Bureau of Ships
Department of the Navy
Washington 25, D. C.
(2)Attn: Code 312
(2) 430
(2) 550
(1) 590
(1) 513
(1) 551
(1) Director of Research

Chief, Bureau of Aeronautics
Department of the Navy
Washington 25, D. C.
(1)Attn: Aer-AE-651
(2) PP-22
(2) PP-33

Director
Naval Research Laboratory
Washington 25, D. C.
(6)Attn: Code 2028

Naval Engineering Exp. Station
Annapolis, Maryland
(6)Attn: Arthur H. Senner

U.S. Naval Postgraduate School
Monterey, California
(1)Attn: Library
(1) Prof. Paul Pucci
(1) Prof. C. P. Howard

(1)Office of the Asst. Chief of Staff, G-4
Research and Development Div.
Department of the Army
Washington 25, D. C.

Armed Services Technical Information Agency
Arlington Hall Station
Arlington 12, Virginia
(10)Attn: DSC

U.S.Army Ordnance Missile Command
Army Ballistic Missile Agency
Redstone Arsenal, Alabama
(1)Attn: ORDAB-RRT

U.S.Atomic Energy Commission
Plans and Analysis Branch
Washington 25, D. C.
(1)Attn: Major J.D.Radcliff,USAF

U.S.Atomic Energy Commission
Division of Reactor Development
Washington 25, D. C.
(1)Attn:Chief, Reactor Component Development Branch
(1) Mr. Nordlinger

(1)U.S.Atomic Energy Commission
Technical Information Service
P.O.Box 62
Oak Ridge, Tennessee

Director
Engineering Res.and Dev.Lab
Fort Belvoir, Virginia
(1)Attn: Head,Nuclear Power Branch

U.S.Coast Guard Hq.
Testing and Development Div.
1303 E Street
Washington, D. C.
(1)Attn: W.S.Vaughn, Cdr., USCG

Wright Air Development Center
Wright-Patterson AFB, Ohio
(1)Attn: WCRGO-2
(1) Mr.M.T.Davis,WCLOS

National Aeronautics and Space Administration
Ames Research Center
Moffett Field, California
(2)Attn: Library

National Aeronautics and Space Administration
Langley Research Center
Langley Field
Hampton, Virginia
(1)Attn: Library

National Aeronautics and Space Administration
Lewis Research Center
21000 Brookpark Road
Cleveland 35, Ohio
(1)Attn: Library

(5)Administrator
National Aeronautics and Space Administration
1520 H Street, N.W.
Washington 25, D. C.

Oak Ridge National Laboratory
9204-1, Y-12
P.O.Box Y
Oak Ridge, Tennessee
(1)Attn: Mr. Richard W. Lyon
(1) Technical Library

(1)American Society of Heating and Ventilating Engineers
Research Laboratory
7218 Euclid Avenue
Cleveland 3, Ohio

American Society of Mechanical Engineers
29 West 39th Street
New York 18, New York
(1)Attn: Mrs. D.M.Shackelford, Standards Administrator

(1)Detroit Public Library
Technology Department
96 Putnam Avenue
Detroit 2, Michigan

(1)Engineering Societies Library
United Engineering Trustees,Inc.
29 West 39th Street
New York 18, New York

McGraw-Hill Publishing Co.
330 West 42nd Street
New York 36, New York
(1)Attn: Mr. L.N.Rowley, Exec. Editor, POWER

Auburn University
Department of Mechanical Engrg.
Auburn, Alabama
(1)Attn: Prof.Donald Vestal, Chairman

Brooklyn Polytechnic Institute
99 Livingston Street
Brooklyn 1, New York
(1)Attn: Engineering Library

California Inst. of Technology
Mechanical Engineering Dept.
1201 East California Street
Pasadena 4, California
(1)Attn: Mechanical Engrg. Library
(1) Prof. B. H. Sage

University of California
College of Engineering
Berkeley 4, California
(1)Attn: Dean E. D. Howe
(1) Prof. R. A. Seban,M.E.
(1) Prof. H. A. Johnson,M.E.
(1) Prof. A. K. Oppenheim,M.E.

University of California at Los Angeles
Engineering Department
Los Angeles 24, California
(1)Attn: Dean L.M.K. Boelter
(1) Prof. W. J. King
(1) Prof. Myron Tribus
(1) Mr. H. Buchberg

Case Institute of Technology
Dept. of Mechanical Engrg.
University Circle
Cleveland 6, Ohio
(1)Attn: Prof. J. R. Moszynski

The Catholic University of America
Department of Mechanical Engineering
Washington 17, D. C.
(1)Attn: Mr. E. D. Jordan

Columbia University
Heat Transfer Research Facility
P.O.Box 245, Station J.
New York 27, New York
(1)Attn: AEC Contract Custodian

Cornell University
College of Engineering
Dept. of Heat Power Engrg.
Ithaca, New York
(1)Attn: Prof. David Dropkin

University of Houston
Mechanical Engineering Dept.
Houston, Texas
(1)Attn: Prof.D.G.Williams

Illinois Inst. of Technology
Dept. of Mechanical Engrg.
Technology Center
Chicago 16, Illinois
(1)Attn: Heat Transfer Lab

University of Illinois
Mech. Engineering Dept.
Urbana, Illinois
(1)Attn: Prof. S. L. Soo

Lehigh University
Department of Mech. Engrg.
Bethlehem, Pennsylvania
(1)Attn: Prof. Frank Kreith

Massachusetts Inst. of Tech.
Cambridge 39, Mass.
(1)Attn: Prof. Joseph Kaye. Mech. Engrg.
(1) Prof. Harold S. Mickley Chem. Engrg.
(1) Prof. Edward S. Taylor Gas Turbine Lab
(1) Prof. William H. McAdams Chem. Engrg.
(1) Prof. Warren M. Rohsenow Mech. Engrg.

University of Michigan
228 W. Engineering Bldg.
Ann Arbor, Michigan
(1)Attn: Prof. J. A. Clark
(1) Prof. P. L. Schwartz

University of Minnesota
Mechanical Engineering Dept.
Minneapolis, Minnesota
(1)Attn: Dr. E.R.G.Eckert

University of New Mexico
Dept. of Mech. Engineering
Albuquerque, New Mexico
(1)Attn: Prof. V. J. Skoglund

New York University
College of Engineering
Dept. of Mechanical Engrg.
University Heights
New York 53, New York
(1)Attn:Prof. Fred Landis

Princeton University
Princeton, New Jersey
(1)Attn: Prof. R. M. Drake,Jr. Engineering
(1) Library, James Forrestal Research Center
(1) F.L.Arnold, Periodicals Div., Library

Purdue University
School of Mechanical Engrg.
Lafayette, Indiana
(1)Attn: Prof. L. S. Clark

University of Santa Clara
Santa Clara, California
(1)Attn: Prof. R. K. Pefley

Stanford University
Stanford, California
(1)Attn: Dean J. M. Pettit, Sch. of Engrg.
(2) Engineering Library

Syracuse University
Syracuse, New York
(1)Attn: Ralph M. Watson,Asst. Dean of Engrg.

Tufts University
Mechanical Engineering Dept.
Medford 55, Mass.
(1)Attn: Dr. L. M. Trefethen, Chairman

Virginia Polytechnic Inst.
Blacksburg, Virginia
(1)Attn: Carol M. Newman Lib.

University of Washington
College of Engineering
Seattle 5, Washington
(1)Attn: Dean H. E. Wessman

University of Wisconsin
Dept. of Mechanical Engrg.
Madison, Wisconsin
(1)Attn: Prof. Edward Obert

Aerojet-General Corp.
Liquid Engine Division
Azusa, California
(1)Attn: Mr. C. C. Ross

Aerojet-General Nucleonics
Fostoria Way
San Ramon, California
(1)Attn: Library
(1) Dr. D. L. Cochran
(1) Mr. A. V. Licin

The Air Preheater Corp.
Wellsville, New York
(1)Attn: Mr. Hilmer Karlsson, Technical Manager

AiResearch Mfg. Company
9851-9951 Sepulveda Blvd.
Los Angeles 45, California
(2)Attn: Mr. S. K. Andersen
(1) Dr. J. E. Coppage
(1) Mr. A. L. Johnson, Jr.
(1) Dr. John Mason

AiResearch Manufacturing Co.
402 South 36th Street
Phoenix, Arizona
(1)Attn: Mr. S. B. Spangler,Jr.
(1) Elmer Wheeler, Dept. 93-32

Alco Products, Inc.
Dunkirk, New York
(1)Attn: Mr. S. Kopp

Allis-Chalmers Mfg. Co.
General Machinery Div.
Milwaukee 1, Wisconsin
(1)Attn: Mr. R. C. Allen, Dir. of Mech. Engrg.

American-Standard
Advanced Technology Labs
369 Whisman Road
Mountain View, Calif.
(1)Attn: F. Lansing

American Standard Corp.
Industrial Division
8111 Tireman Avenue
Detroit 32, Michigan
(1)Attn: Mr. T. Tinker,V-P, Technical Development

American-Standard Corp.
Industrial Division
P.O. Box 2081
Buffalo 5, New York
(1)Attn: Mr.J.A.Jost,Dir.Res.
(1) Mr.I.R.Friedman,Mgr. Res. Engineering

Argonne National Labs
9700 South Cass Ave.
Argonne, Illinois
(1)Attn: Technical Library
(1) Dr. B. I. Spinrad, Dir.Reactor Engrg.
(1) Dr. David Miller, ISNE School
(1) Mr. M. Petrick

Arnold Equipment Corp.
3080 Main Street
Buffalo 14, New York
(1)Attn: Mr. A. G. Tessmer

Aro, Inc.
Technical Information Branch
Tullahoma, Tennessee
(1)Attn: Mr. G. E. Randall

Atlantic Research Corporation
Alexandria, Virginia
(1)Attn: Dr. M. Markels, Jr.

Atomics International
P.O. Box 309
Canoga Park, Calif.
(1)Attn: Library

Atomic Power Dev. Associates,In
1911 First Street
Detroit 26, Michigan
(1)Attn: Mr. A. Amorosi
(1) Dr. Wayne H. Jens

Avco Research Lab
2385 Revere Beach Parkway
Everett 49, Mass.
(1)Attn: Technical Library

(1)The Babcock and Wilcox Co.
Research and Dev. Center
P.O Box 835
Alliance, Ohio

Battelle Memorial Institute
505 King Avenue
Columbus 1, Ohio
(1)Attn: Dr. A. W. Russell

C. F. Braun and Co.
1000 S. Fremont St.
Alhambra, Calif.
(1)Attn: Mr. Karl Gridizze

Brookhaven National Laboratory
Technical Information Division
Upton, Long Island, New York
(1)Attn: Research Library

Brown Boveri Corp.
19 Rector St
New York 6, New York
(1)Attn: Mr.F.R.Sidler,Pres.

Brown Fintube Co.
300 Huron St.
Elyria, Ohio
(1)Attn: Mr.John W.Brown,Jr.

California Research Corp.
Richmond, Calif.
(1)Attn: Dr.J.H.Macpherson

Carrier Corporation
300 South Geddes St.
Syracuse 1, N. Y.
(1)Attn: Engineering Lib.

Caterpillar Tractor Co.
Peoria 8, Illinois
(1)Attn: Mr.H.S.Eberhard,Pres
(1) Mrs.M.H.Landuyt, Res. Library
(1) Mr. Lloyd E. Johnson

Chrysler Corporation
Automotive Research,
Dept. 981
12843 Greenfield Ave.
Detroit 27, Michigan
(1)Attn: Mr.A.Charlamb, Res. Engineer

Cooper Bessemer Corp.
Mt. Vernon, Ohio
(1)Attn: Mr.R. L. Boyer, Vice Pres.

Cornell Aeronautical Lab.
4455 Genesee St.
Buffalo 21, New York
(1)Attn: Elma T.Evans,Librarian
(1)Detroit Edison Co.
Nuclear Power Division
Detroit, Michigan

Cosmodyne Corporation
5300 West 104th Street
Los Angeles 45, California
(1)Attn: Albert B. Seed, Project Manager, Applications

Drayer-Hanson, Inc.
Box 2215 Terminal Annex
Los Angeles 54, Calif.
(1)Attn: Mr. Gordon H.Jackson, Vice President

Eitel-McCullough, Inc.
798 San Mateo Ave.
San Bruno, Calif.
(2)Attn: Mr. J.S.McCullough, Mgr. Research

Electric Boat Company
Groton, Connecticut
(1)Attn: Mr.E.S.Dennison

Elliott Company
Jeannette, Pennsylvania
(1)Attn: Mr. J.Rodger Shields, Dev.Engrg.Dept.

Fairchild Engine and Airplane Corporation
Fairchild Astrionics Div.
Wyandanch, Long Island,N.Y.
(1)Attn: Alex London, Sr. Engineer,Aero-mechanics Div.

Fairchild Engine and Airplane Corp.
Stratos Division
Bay Shore, Long Island,N.Y.
(1)Attn: Mr.V.L.Whitney,Jr. Res. Engineer

Ferrotherm Company
1861 E. 65th Street
Cleveland 3, Ohio
(2)Attn: Mr. Sven Holm

The Fluor Corp. Ltd.
Research and Dev. Div.
P.O.Box 510
Whittier, Calif.
(1)Attn: Mr.C.L.Blohm, Mgr. Research

Ford Motor Company
Dearborne, Michigan
(1)Attn: Mr.Paul Klotsch, Res. Div.
(1) Dr.D.N.Frey, Scientific Lab
(1) Mrs.Rachel MacDonald, Eng.Staff Library
(1) Mrs.L.B.Phillips, Superintendent, Tech.Info.Sec., Scientific Lab

Foster Wheeler Corp.
165 Broadway
New York 6, New York
(1)Attn: Mr. John Blizard, Dir. Res. and Engineering

The Franklin Institute
Laboratories for Research and Development
Philadelphia 3, Pa.
(1)Attn: Mr.F.L.Jackson

General Dynamics Corp.
General Atomic Division
P.O. Box 608
San Diego 12, Calif.
(1)Attn: F.W.Slepern, Document Custodian

General Electric Company
Atomic Power Equipment Div.
San Jose, California
(1)Attn: W. A. Sutherland
(1) F. E. Tippetts

General Electric Company
Cincinnati 15, Ohio
(1)Attn: Mr. M. E. Lapides, Aircraft Nuclear Propulsion Dept.

General Electric Company
General Engineering Lab
Schenectady 5, New York
(1)Attn: Mrs.D.F.Buckland
(1) Dr. J. H. Morris, Thermal Systems Engrg.
(1) D.L.Brown, Thermal Systems Engrg.

General Electric Company
Design Section, Energy Dept.
Richland, Washington
(1)Attn: Mr. Gardner L. Locke

General Electric Company
Small Aircraft Engine Dept.
1000 Western Avenue
West Lynn 1, Mass.
(1)Attn: R.A.Harmon,Marine
Industrial Market
Development

(1)General Metals Corp.
Enterprise Division
19th and Florida Sts.
San Francisco, California

General Motors Corp.
Allison Division
Indianapolis 6, Indiana
(1)Attn: Mr. H. M. Hazen,
Dir. of Engrg.

General Motors Corp.
Research Laboratories
12 Mile and Mound Roads
Warren, Michigan
(1)Attn: Mr.W.A.Turunen, Gas
Turbine Dept.
(1) C. V. O. Smith

General Motors Corp.
Harrison Radiator Div.
Lockport, New York
(2)Attn: Mr. John W. Godfrey

General Nuclear Engineering
Corporation
Dunedin, Florida
(1)Attn: Ray L. Lyerly, Staff
Engineer
(1) Librarian

The Grisco-Russell Company
285 Madison Avenue
New York 17, New York
(1)Attn: Mr. George Root,
Chief Engineer

Gulf Oil Corp.
Gulf Building
Pittsburgh 30, Pennsylvania
(1)Attn: Mr. Charles F. Kottcamp

The Heat-X-Changer Co., Inc.
Brewster, New York
(1)Attn: Mr. W. J. Donovan,
Vice President

Hughes Aircraft Company
Florence and Teale Sts.
Culver City, California
(1)Attn: Dana H. Johnson, Dir.
Technical Library

Ingersoll-Rand Company
11 Broadway
New York, New York
(1)Attn: Mr. M. C. Davison

International Harvester Co.
Engineering Research Dept.
5225 S. Western Blvd.
Chicago 9, Illinois
(1)Attn: Dr. Simon K. Chen

I-T-E Circuit Breaker Co.
601 E. Erie Avenue
Philadelphia 34, Pa
(1)Attn: Mr. Ashton T. Scott

Jack and Heintz, Inc.
Engineering Dept., Plant 8
Cleveland 1, Ohio
(1)Attn: Mrs. Harriet B. Trikilis,
Librarian

M. W. Kellogg Company
711 Third Avenue
New York 17, New York
(1)Attn: Mr. P. W. Peterson
(1) Mr. O. P. Hachenbrenner
(1) Mr. Ronald B. Smith,
Vice President

The Kreisel Co., Inc.
229 Williams Avenue
Hackensack, New Jersey
(1)Attn: Mr. F. Kreisel, Jr.

Lockheed Aircraft Co.
Technical Library
Burbank, California
(1)Attn: B. L. Messinger,
Engrg. No. 7225

Lockheed Aircraft Corp.
Missile Systems Division
Aerodynamics Dept.
Sunnyvale, California
(1)Attn: Mr. O. A. Stenad

Lummus Company
186 Haynes Avenue
Newark, New Jersey
(1)Attn: Stanley Grossel,
Process Engineer

McCulloch Motors Corp.
6101 West Century Blvd.
Los Angeles 45, Calif.
(1)Attn: W. K. Dawson, Chief
Engr., Aircraft
Engines

Thos Marquardt Corp.
Controls and Accessories Div.
16655 Setticoy Street
Van Nuys, California
(1)Attn: Robert T. Lanest

Glenn L. Martin Company
Baltimore 3, Maryland
(1)Attn: Mr. T. F. Hagey,
Project Engineer

Micro-Precision Inc.
Engineering Department
2105 Lee Street
Evanston, Illinois
(1)Attn: Mr. Louis D. Kaplan

Mine Safety Appliances Co.
Callery Plant
Callery, Pennsylvania
(1)Attn: Dr. C. B. Jackson

Nesbitt Manufacturing Co.
1500 DeKoven Avenue
Racine, Wisconsin
(1)Attn: Mr.C.T.Perkins,Pres.

Morgantown Research Center
Bureau of Mines
Morgantown, West Virginia
(1)Attn: Mr.J.P.McGee

North American Aviation,Inc.
International Airport
Los Angeles 45, Calif.
(1)Attn: Mr. H. A. Sulkin

Perfex Corporation
5600 West Oklahoma Avenue
Milwaukee 7, Wisconsin
(1)Attn: Mr. W. W. Schwid

Sanderson and Porter
72 Wall Street
New York 5, New York
(1)Attn: Mr.S.T.Robinson

Shell Development Company
Emeryville, California
(1)Attn: Dr. L. M. Garbett

S. O. Smith Corp.
3533 North 27th Street
Milwaukee 1, Wisconsin
(1)Attn: Mr. M. E. Ziering

Solar Aircraft Company
San Diego 12, California
(2)Attn: Mr.P.A.Pitt, Chief
Engineer
(1) Mr. E.A.Drury,Project
Engineer,Dept.222

Stalker Development Co.
903 Woodside Avenue
Essexville, Michigan
(1)Attn: Mr. E.A.Stalker

Stanford Research Institute
Menlo Park, California
(1)Attn: Dr. Nevin K. Hiester
(1) Mr. S. H. Clark
(1) Mr. W. A. Casler

Stewart-Warner Corp.
1514 Drover Street
Indianapolis 7, Indiana
(2)Attn:Mr.M.D.Randall,
Mgr. Research

Sulzer Bros. Ltd
50 Church Street
New York 7, New York
(1)Attn: Mr. Richard Herold

(1)Sverdrup and Parcel, Inc.
Syndicate Trust Bldg.
St. Louis 1, Missouri

Sylvania Electric Products,Inc.
Electronic Defense Lab
P.O. Box 205
Mountain View California
(1)Attn: Librar

Texas Eastern Transmission
Corp.
P.O.Box 1612
Shreveport, Louisiana
(1)Attn: Mr. C. W. Marvin

The Trane Company
2nd and Cameron Avenues
La Crosse, Wisconsin
(2)Attn: Mr. M. C. Rooks
(1) Mr. I. T. Wetzel

(2)Union Carbide Nuclear Co.
Oak Ridge Gaseous Diffusion
Plant
Plant Records Department
P. O. Box P
Oak Ridge, Tennessee

United Aircraft Corp.
400 Main Street
East Hartford 8, Conn.
(1)Attn: Mr. Robert C. Sale,
Chief Librarian
(1) Mr. Ned C. Rice, Jr.,
Research Dept.

Vidya Inc.
2626 Hanover Street
Palo Alto, Calif.
(1)Attn: M.W.Rubesin
(1) D.E.Abbott
(1) D.C.Briggs

Western Supply Co.
P. O. Box 1868
Tulsa 1, Oklahoma
(1)Attn: Mr.E.D.Anderson,
Chief Engineer

Westinghouse Electric Corp.
Lester Branch P. O.
Philadelphia 13, Pa.
(1)Attn: Mr.F.K.Fischer,Mgr.
Dev. Engrg.

Westinghouse Electric Corp.
Apparatus Department
P. O. Box 1526
Pittsburgh, Pennsylvania
(1)Attn: Mr. Abner Sacks

Westinghouse Electric Corp.
Atomic Power Division
P. O. Box 1468
Pittsburgh 30, Pa.
(1)Attn: Technical Library

Westinghouse Electric Corp.
Research Laboratory
East Pittsburgh, Pa.
(1)Attn: Dr. Stewart Way

Wolverine Tube Division
1411 Central Avenue
Detroit 9, Michigan
(1)Attn: Mr.J.S.Rodgers,
Technical Mgr.

Worthington Corp.
Harrison Division
Harrison, New Jersey
(1)Attn: Mr. Normen L.
Myerson,Dir. of
Research
(1) Mr. David Aronson

Young Radiator Company
709 S. Marquette St.
Racine, Wisconsin
(1)Attn: Mr. H.P.Brinen,
Res. Engineer

Yuba Consolidated Industries,
1 Bush Street
San Francisco, California
(1)Attn: K.A.Gardner, Vice Pres.,
Engineering

(1)Mr. Hector H. Aiken
904 Willow Road
Menlo Park, Calif.

(1)Dr. W. Bolley
Hope Ranch
Santa Barbara, Calif.

(1)Mr. F. A. Brooks
Dept. of Agr. Engrg.
Univ. of Calif. Agr.
Experiment Station
Davis, California

(1)Prof. Alberto Coimbra
Escola Nacional de Quimica
Av. Pasteru 404
Rio de Janeiro, BRASIL

(1)Mr. W. H. Comtois
29 Brentwood Drive
Bloomfield, Connecticut

(1)Mr. Paul Dawson
8320 East Galbraith
Cincinnati 43, Ohio

(1)Mr. A. J. Ede
Heat Division
Mech. Eng. Research Lab
D.S.I.R., East Kilbride
near Glasgow, SCOTLAND
SEND TO:
Office of the Asst. Naval
Attache for Research
Naval Attache, American
Embassy
Navy No. 100, Fleet P. O.
New York, New York

(1)Mr. C. H. Fixman
Chief Marine Engineer
Code 254
San Francisco Naval
Shipyard
San Francisco 25, Calif.

(1)Dr. Robert W. Fox
Dept. of Mech. Engrg.
Purdue University
Lafayette, Indiana

(1)Mr. Ralph M. Heintz
P. O. Box 546
Los Gatos, Calif.

(1)Mr. Albert L. Holiday
550 Lakewood Circle
Walnut Creek, Calif.

(1)Mr. Robert V. Kleinschmidt
20 East Street
Stoneham 80, Mass.

(1)Dr. Milton B. Larson
Dept. of Mech. Engrg.
Oregon State College
Corvallis, Oregon

(1)Rear Adm. Paul F. Lee,
USN Ret.
18975 Manuella Avenue
Los Altos, Calif.

(1)Mr. E. J. Le Fevre
Department of Mechanical
Engineering
Queen Mary College
London E. 1, ENGLAND

(1)Dr. J. J. McMullen
1114 Clinton Street
Hoboken, New Jersey

(1)Mr. Frank L. Maker
156 Moraga Highway
Orinda 1, California

(1)Dr. Carl A. Moore, Jr.
3307 Sunnywood Drive
Fullerton 1, California

(1)Mr. A. J. Oberg
Minneapolis-Honeywell
Regulator Company
Research Center
500 Washington Ave., So.
Hopkins, Minnesota

(1)R.C.Perpall
5453 Whitefox Drive
Palos Verdes Estates
California

(1)Major Walter E. Rafert
Asst. Prof. - Armament
Dept. of Ordnance
U.S.Military Academy
West Point, New York

(1)Mr. L.F.Saunders
P. O. Box "L"
Carmel, Calif.

(1)Mr.David M.Schoenfeld
Mariomi Road
New Canaan, Conn.

(1)Mr. Edward Simons
355 Taraval St.
San Francisco 16,Calif.

(1)Mr. Richard L. Stone
William Wallace Co.
Belmont, Calif.

(1)Mr. Stanley Wong
1128 West 126th Street
Los Angeles 44, Calif.

(1)Dr.J.G.Woodroof,
Chairman
Food Processing Div.
Georgia Exp. Station
Experiment, Georgia

Best Available Copy